Archaean gold mineralisation during post-orogenic extension in the New Consort Gold Mine, Barberton Greenstone Belt, South Africa

M. Richard Munyai[1,3], Paul H. G. M. Dirks [1,2], and E. Guy Charlesworth[1]

[1] *School of Geosciences, University of the Witwatersrand, Private Bag 3, Johannesburg, 2050, South Africa*

[2]*School of Earth and Environmental Science, James Cook University, Townsville, Qld 4811, Australia*

[3]Corresponding author: e-mail: mphoyanga@yahoo.com

ABSTRACT

The area around New Consort Gold Mine (NCGM) is complexly deformed during at least 5 distinct events named D_{1NC} – D_{5NC}. D_{1NC} - D_{3NC} events involve progressive shearing and folding linked to the 3250-3225 Ma accretionary history of the Barberton greenstone belt (D_{1NC} and D_{2NC}), and subsequent 3105 Ma emplacement and doming of surrounding batholiths (D_{3NC}). During D_{3NC} the area experienced intense strain partitioning with the development of a network of shear zones, which envelop structural domains characterised by locally unique deformation histories. Around NCGM, D_{3NC} events involved early shearing (D_{3aNC}) along the Consort Bar followed by two episodes of 600m scale folding (D_{3bNC} and D_{3cNC}) resulting in a complex fold interference pattern. Pegmatites intruded during D_{3NC}. D_{4NC} structures comprise a network of extensional brittle-ductile shear fractures and associated kink bands and crenulation folds that formed concomitant with gold mineralisation after all the D_{3NC} structures had fully developed, marking a clearly separate event. The D_{4NC} fractures are distributed along 100-200m wide corridors as 10-100m scale, en-echelon, Riedel, anti-Riedel and P-shear arrays. D_{5NC} structures represent late reverse faults of unknown age.

The critical structures controlling gold mineralisation are the D_{4NC} fracture zones. The distribution of high-grade ore zones is controlled by the intersection orientation of D_{4NC} fractures and suitable host lithologies, mainly the silicified hinge zones of D_{1NC} folds and the laminated chert of the Consort Bar. Because these host lithologies were complexly folded in D_{1NC}-D_{3bNC}-D_{3cNC} fold interference patterns, the 3-D distribution of ore zones is highly discontinuous and complex.

Kinematics analysis and stress inversion using Bingham tensor solutions and an optimized dihedron method, of mineralised D_{4NC} fractures along old gold workings at NCGM, consistently indicate a vertical σ_1, and a horizontal NW-SE directed σ_3, within a pure extensional stress regime indicating that gold mineralisation occurred in an extensional tectonic setting. Results for the nearby Clutha, Albion and Woodstock mines are similar. This study suggests that gold mineralisation in the NCGM area can be linked to an extensional event that may have developed separately from the accretionary events shaping the craton and may have coincided with the opening of Dominion Group basins.

Introduction

Lode gold deposits are an important type of gold mineralisation in orogenic settings around the world and through time (e.g. Goldfarb *et al.*, 2001). They are structurally controlled and commonly associated with second-order structures near major brittle-ductile shear zones developed in Archaean greenstone belts (Condie, 1981; Robb, 2004; Groves *et al.*, 1998). The formation of lode gold deposits has been linked to tectonically active plate boundary zones (Groves *et al.*, 1998; Goldfarb *et al.*, 2001), with controlling thrusts and strike-slip faults formed in accretionary settings (de Ronde and de Wit., 1994). Mineralised shear zones are commonly reactivated repeatedly to give rise to complex mineralisation patterns (Sibson, 2001, 2004).

The 3.6-3.1 Ga Barberton Greenstone Belt (BGB) in the Kaapvaal Craton of South Africa, is an Archaean greenstone terrain interpreted as an accretionary arc sequence (e.g. de Ronde and de Wit, 1994) hosting numerous gold deposits (Anhaeusser 1969, 1976, Ward, 2000). Since 1885, the belt has produced more than 345 tons of gold (Dirks *et al.*, 2009), leaving behind numerous old workings, pits and shafts that provide excellent access for detailed studies on mineralisation controls. Gold in the BGB has been linked to large accretionary thrust zones that were reactivated as brittle-ductile, strike-slip faults and thrusts during the rise of large granite plutons such as the 3106 Ma Nelspruit Batholith (Anhaeusser, 1976; de Ronde and de Wit., 1994; Harris *et al,* 1995; Ward, 2000), presumably during the last stages of accretionary formation of the BGB (de Ronde and de Wit, 1994). In contrast, Dirks *et al*. (2009) have shown that mineralisation in the Sheba area, including the world class Sheba and Fairview deposits, was controlled by a network of normal brittle-ductile shear zones, fractures and faults that formed in an intracratonic, post-orogenic, extensional environment, which they suggest was unrelated to accretion of the greenstone sequence.

Most gold mined in the BGB comes from four mines: Agnes, New Consort, Fairview and Sheba Gold Mines, which collectively produced 80% of all gold produced in the BGB (Dirks *et al.*, 2009). The New Consort Gold Mine (NCGM), which forms the focus of this study is located in a triple junction area, where greenstones of the

Jamestown Schist Belt (JSB) merge with the main BGB. Gold mineralisation in the NCGM is generally high grade (12-15g/t), and ore zones are complex and commonly discontinuous, and affected by several generations of overprinting folds, brittle-ductile shear zones, faults and pegmatite intrusions, all of which influenced the ore body geometry (e.g. Viljoen, 1964; Anhaeusser, 1976; Voges, 1986; Harris *et al.*, 1995). This complexity has made mine-scale predictive modelling extremely difficult.

The aim of this study is to provide a detailed analysis of the structural history of the NCGM area, focussing on the sequence of ductile and brittle-ductile deformation events that resulted in the complex architectural framework hosting mineralisation. Numerous surface workings scattered around the hills near NCGM, provide observational windows to mineralised zones that are part of a complex network of brittle-ductile shear zones, which interact with the older ductile structures to control gold deposition (e.g. Dirks *et al.*, 2009). In this paper, we aim to describe these controlling structures, their kinematic framework and the nature of the palaeo-stress environment during which they were infiltrated by gold-bearing fluids. The resultant constraints on the tectonic setting of gold mineralisation will be discussed.

Regional geological setting

The Barberton greenstone belt (BGB) represents one of the best preserved mid-Archaean supracrustal sequences in the world. The 40x120km large belt consists of tectonically and stratigraphically interleaved, NE-striking 3.55-3.22 Ga volcanic and clastic rocks surrounded by granite-gneiss domes ranging in age from 3.5-3.1 Ga (Lowe and Byerly, 2007; Fig. 1).

The volcano-sedimentary sequence of the BGB has been subdivided into three lithostratigraphic units from bottom to top: the Onverwacht, Fig Tree and Moodies Groups (Viljoen and Viljoen, 1969; Anhaeusser, 1976; Brandl *et al.*, 2006). The Onverwacht Group is composed of ultramafic to mafic volcanic rocks with minor felsic volcanic flows, tuff and sediments, which formed in a shallow marine environment between 3.55 Ga and 3.26 Ga (Byerly *et al.*, 1996; Lowe and Byerly, 2007). The

overlying Fig Tree Group consists of deep- to shallow-marine turbiditic greywacke, shale and mudstone interbedded with minor chert, banded iron formation (BIF) and felsic volcanic units, deposited in response to erosion of uplifted portions of older greenstone successions (Condie *et al.*, 1970; Hofmann, 2005). Their age is bracketed by volcanics at the base and top dated at 3259+/-5 Ma and 3225+/-3 Ma respectively (de Ronde *et al.*, 1991; Kröner *et al.*, 1992). The volcaniclastic unit at the top of the Fig Tree Group is called the Schoongezicht Formation (Anhaeusser, 1969; Hofmann, 2005). The Moodies Group consists of shallow marine to fluvial sequences of conglomerate, quartzose to feldspathic sandstone and shale with minor BIF and volcanic units deposited after 3226 +/-1 Ma (Kamo and Davis, 1994). A minimum age of deposition obtained from detrital zircon from Moodies sediment is ~3160 Ma (de Ronde and de Wit, 1994).

Structural boundaries divide the BGB into tectonic domains across which the Onverwacht and Fig Tree Group rocks change in terms of stratigraphy, age, depositional environment and deformation history. A major tectonic boundary is the Inyoka-Saddleback fault (Fig. 1) interpreted as a 3226 Ma suture zone (*e.g.* de Ronde and de Wit, 1994). South of the Inyoka-Saddleback fault, Onverwacht Group rocks are 3460-3260 Ma in age and reach a stratigraphic thickness of approximately 10 km, whilst mafic to ultramafic sequences north of the Inyoka fault are thinner (< 1km) and younger at 3330-3240 Ma (Lowe and Byerly, 2007). The Inyoka-Saddleback fault similarly divides the Fig Tree sediments into a southern facies consisting of shallow water and alluvial greywacke sandstone, and a northern facies of deep-water clastic rocks (Hofmann, 2005), whilst Moodies Group rocks tend to be coarser grained south of the Inyoka fault in contrast to those north of the fault.

De Ronde and de Wit (1994) provide a tectonic summary for the evolution of the BGB and place the locally complex, polyphase deformation history of the belt in a simple deformation scheme and make comparisons to modern plate tectonic settings (Table 1). Following the deformation scheme of de Ronde and de Wit (1994), the earliest event, D_0, (3490-3450 Ma) represents alteration processes near oceanic volcanic spreading centres (ridges; <3460Ma) and involved extension. A later (3450-3416 Ma) thermo-tectonic event, D_1, resulted from subduction-like processes with emplacement of proposed ophiolite allochtons in intra-oceanic environments and the emplacement of TTG plutons.

A second phase of subduction-accretion, D_2, between 3260-3225 Ma, likened to an Andean margin setting, was accompanied by inter-arc deformation and culminated in accretion of unrelated arc systems around 3225 Ma, with the Saddleback-Inyoka fault system identified as the dominant suture. Convergence and accretion followed by post-accretionary, transpressional events grouped as early-D_3, continued between 3225-3126 Ma, and resulted in the NE-trending map pattern of the BGB and the formation of strike-parallel faults linked to gold mineralization (de Ronde *et al.*, 1991, Ward, 1999). Gold mineralization occurred as part of late D_3 events between 3126+/-26 Ma and 3084+/-18 Ma (de Ronde *et al.*, 1992), coinciding with a shift from transpressional to transtensional tectonics. Regional extensional collapse, termed D_4 (de Ronde and de Wit, 1994), around 3100 Ma accompanied by the emplacement of potassic granite batholiths, post-dated mineralisation and preceded cratonic stabilization (e.g. Dirks and Jelsma, 1998; Table 1).

More detailed deformation schemes are available for the SW BGB (*e.g.* Lowe, 1994; Lowe *et al.*, 1999), and for the Sheba-Fairview gold mine area (Dirks *et al.*, 2009), where thrusts that separate tightly folded rocks of the Fig Tree and Onverwacht Groups from more open, but similarly orientated, folds in the Schoongezicht Formation and overlying Moodies Group have been described (Fig. 1). Dirks *et al.* (2009) note that the Fig Tree and Onverwacht rocks were folded before deposition of the Schoongezicht Formation and Moodies Group and refer to pre-Moodies Group folding of Fig Tree rocks as D_1 (= D_2 of Lowe *et al.*, 1999) to shearing along the Fig Tree-Moodies contact rocks and simultaneous folding of the Moodies Group rocks (and tightening of D_1 folds in Fig Tree lithologies) as D_2, refolding of the D_2 folds in the Moodies as D_3 and subsequent recumbent folding, kink folding and normal faulting as D_4, in part following older deformation schemes proposed by Ramsay (1963) and Anhaeusser (1976) (Table 1).

Geology of the New Consort Gold Mine

The New Consort Gold Mine (NCGM) is located in a triple junction area of the BGB, where the NW trending Jamestown Schist Belt (JSB) merges with the NE trending main branch of the BGB (Fig. 1). The 3106±3 Ma (Kamo and Davis, 1994) Nelspruit Batholith including gneiss of the 3107±5 Ma Stentor pluton (Kamo and Davis, 1994), and

the 3227±1 Ma (Kamo and Davis, 1994) Kaap Valley Pluton bound this triple junction to the N and SW respectively (Fig. 1). These plutons have acted as buttresses between which the complex constrictional structures that characterise the NCGM area were formed. To the SE, the triple junction area is bounded by a thick sequence of clastic sediments belonging to the Moodies Group that have been folded in a large synclinal structure called the Eureka Syncline (Fig. 1).

The NCGM area is transected by a series of major shear zones including the Lily, Albion, Woodstock and Kaap River Faults (Fig. 1), which act as boundaries to structural domains with distinct deformation and metamorphic histories (e.g. Anhaeusser, 1976; Dziggel *et al.*, 2007). The Kaap River Fault forms the southern boundary of complexly folded greenschist to amphibolite grade rocks that host the gold mineralisation around the NCGM (Fig. 1).

Gold mining in the NCGM area started in 1886 on the Ivaura and MMR sections (Fig. 2). In the early days of mining, numerous surface workings were developed, many on small and discontinuous ore zones, resulting in hundreds of small workings scattered around the NCGM area. As mining progressed, activity focused on a limited number of major shoots including the No.7 Shaft, the Ivaura, the MMR and PC shoots, which have been mined down to 1600 m level (Voges, 1986) resulting in a total production to date of 68.5 tons of gold (Dirks *et al.*, 2009).

Rocks of the Onverwacht, Fig Tree and Moodies Groups in the NCGM (Fig. 2), have been described in detail by Viljoen (1964) and Anhaeusser (1976). Onverwacht Group rocks constitute the bulk of the JSB and comprise komatiitic, and tholeiitic basalt sequences intruded by layered intrusive mafic-ultramafic complexes collectively grouped as the 3.286 Ga Weltevreden Formation (Byerly *et al.*, 1996; Lowe and Byerly, 1999).

These rocks have been deformed and metamorphosed resulting in a complex patchwork of massive, relatively undeformed, lensoidal bodies of ultramafic rocks, including dunite and pyroxenite, surrounded by highly strained, schistose units of variable composition ranging from serpentinite, via talc-carbonate-chlorite schist to amphibolite (Viljoen, 1964). Hornblende-rich amphibolite is common near the contact between the greenstones and the Nelspruit Batholith reflecting an amphibolite facies contact metamorphic aureole along the northern margin of the JSB (Viljoen, 1964).

The top of the Onverwacht Group consists of a 1-25 m thick laminated chert horizon called the Consort Bar, which is the equivalent of the Zwartkoppie Formation in the Sheba area (Anhaeusser, 1976). The Consort Bar is a fine-grained, banded, fuchsite-bearing chert (Hearn, 1943; Voges, 1986), with diopside-rich skarn alteration along its footwall contact that formed, at least in part, as a result of alteration and silicification of ultramafic rocks (Schouwstra and de Villiers, 1988). The overlying Fig Tree Group is composed of thinly bedded, greywacke sandstone and shale units, that are strongly foliated and in places, tightly folded.

The Onverwacht and Fig Tree Group rocks are unconformably overlain by dacitic tuffs, and agglomerates of the Schoongezicht Formation. The agglomerate typically contains rounded dacite pebbles with diffuse boundaries embedded in an amphibole-bearing, dacitic tuffaceous matrix, rich in mm-scale plagioclase crystals. The agglomerate grades into a polymict conglomerate of the overlying Moodies Group (Viljoen, 1964; Anhaeusser, 1969), which outcrops to the W and SE of NCGM (Fig. 2). The conglomerate contains flattened black and jaspillitic chert, granite and vein quartz pebbles set in a medium-grained micaceous quartzite matrix. Moodies Group conglomerate is overlain by a thickly bedded quartzite unit preserving cross-bedding (Viljoen, 1964), which grades into thinly bedded arkose preserving trough cross-bedding. The stratigraphy for the NCGM conforms closely with that observed in the Sheba area to the south of the Lily Fault (e.g. Anhaeusser, 1976; Dirks *et al.*, 2009).

Rock units around the NCGM are complexly folded, and the detailed deformation history for the NCGM compiled by Ramsay (1963) and Viljoen (1964) and summarised in Anhaeusser (1976) has remained the standard reference framework for the area, with local, mine-based adjustments to the deformation history reported in abstracts and mine reports (e.g. Tomkinson and Lombard, 1990); even though tectonic interpretations of the structure have evolved (e.g. Harris *et al.,* 1995; Dziggel *et al.*, 2007). Viljoen (1964) describes a D_1 event that involved tight folding of the Onverwacht, Fig Tree and Moodies Groups linked to the formation of the Eureka Syncline to the south (Anhaeusser, 1976). Following Ramsay (1963), Viljoen (1964) interpreted D_2 as resulting in the formation of a regional cleavage and a stretching lineation including pebble elongation in Moodies Group conglomerate. D_3 resulted in complex folding of the Consort Bar around the large,

SE plunging synclinorium (Viljoen, 1964; Voges, 1986). Viljoen (1964) linked D_3 to diapiric doming of the Nelspruit Batholith and to gold mineralization. Dziggel *et al.* (2007) added detail to the D_1-D_3 events of Viljoen (1964) by providing kinematic information for D_1/D_2 fabrics interpreted as N-up shear fabrics linked to doming of the Stentor Pluton. Mylonites, which occur along the Consort Bar, have been interpreted by Dziggel *et al.* (2007) as syn-D_3, and formed during extension allowing rapid exhumation of higher metamorphic grade rocks from below the Consort Bar. D_4 recumbent folds and horizontal crenulations were observed throughout the area (Viljoen, 1964) and linked to conjugate folds and kink-bands related to late tectonic normal faulting described in detail by Anhaeusser (1976).

Tomkinson and Lombard (1990) in an unpublished abstract documented the presence of a NW trending shear system with mylonite and ultramylonite zones crossing the central part of the NCGM, and called this system the Shires Shear Zone. This observation was based on underground exposures, but no such shear zone can be mapped or has been observed on surface, and the validity of this structure is unclear, despite the fact that it has been adopted in several later papers (e.g. Harris *et al.*, 1995; Dziggel *et al.*, 2007; Otto *et al.*, 2007).

The area around NCGM has been affected by several metamorphic events that vary in grade across the shear zone-bounded domains around the mine. A contact metamorphic aureole affecting rocks along the northern margin of the JSB was recognised by Viljoen (1964). Peak metamorphic conditions were achieved during D_1 in Onverwacht Group schist near the southern margin of the Stentor Pluton and north of the Consort Bar (Dziggel *et al.*, 2006). These conditions have been variably (and confusingly) reported as 600-700 °C, 5+/- 1 kbar (Dziggel *et al.*, 2006) and 600-700 °C, 6-8 kbar (Otto *et al.*, 2007) for garnet-sillimanite-bearing metapelitic and garnet-hornblende-clinopyroxene-bearing metabasic assemblages respectively. Peak conditions drop sharply to 510-530 °C at 4 kbars in Fig Tree Group rocks west of No 3 shaft. A second metamorphic event recorded around the mine, also shows an increase in grade from No 3 shaft in the SW to PC shaft in the NE (Fig. 2) from 530+/-20 °C at 4-5 kbar to 590+/-20 °C at 4-5 kbar respectively (Dziggel *et al.*, 2006; Otto *et al.*, 2007). This event was tentatively linked to shearing along the Consort Bar and gold mineralisation, and to

the emplacement of pegmatite veins (Harris *et al.*, 1995). A third, retrograde, lower greenschist facies metamorphic event has been linked to alteration assemblages along late, cross cutting faults.

Muscovite-bearing pegmatite bodies are common along the folded Consort Bar and the northern extremes of the JSB towards the margin of the Nelspruit Batholith, to which they have been linked on geochemical grounds (Harris *et al.*, 1995; Harris, 1992). Regional fractionation trends in lithium-rich pegmatite bodies reflect increased metamorphic conditions at deeper levels in the mine and towards the NE, with crystallisation conditions reported at 500-650 °C and 3-4 kbar, and coinciding with gold mineralisation (Harris *et al.*, 1995).

The complexity of the geology around the NCGM has resulted in variable interpretations for gold mineralisation, and its timing. All studies agree that gold mineralization was structurally controlled (e.g. Viljoen 1964; Voges, 1986; Harris *et al.*, 1995; Dziggel *et al.,* 2007), but there remains a paucity of detailed structural information on the exact controls.

The main ore shoots occur in amphibolitic schist of the Onverwacht Group in the immediate footwall of the folded Consort Bar and along the bar itself (e.g. No7, Ivaura, MMR and PC shoots), with minor ore shoots occurring in Fig Tree meta-greywacke and chert units in the hanging wall of the Consort Bar (e.g. Hard Cash, Shires and Betty's Quarry shoots), as well as in schist and deformed felsic porphyry deeper into the footwall (e.g. Witkoppies and Bluejackets ore shoots; Fig. 2; Voges, 1986; Ward, 1999). Ore bodies occur as 10-80 m wide, SE and SW plunging ore shoots that are sub-parallel to the orientation of the Consort Bar, and in places transgress the bar. Some ore envelopes can be traced down plunge, as near-continuous ore zones to depths of up to 1600 meters (Voges, 1986; Ward, 1999), and consist of irregular, discontinuous ore shoots cross-cut and displaced by pegmatite bodies (Harris *et al.*, 1995).

D_1 amphibolite containing clinopyroxene-hornblende-garnet-feldspar-biotite in the footwall of the Consort Bar has been (tentatively) linked to an early stage of gold mineralisation (e.g. Otto *et al.*, 2007). In general, mineralisation is thought to be late and related to the dominant D_3 fold and shear structures (e.g. Viljoen, 1964; Voges, 1986; Tomkinson and Lombard, 1990), and mineralising fluids have been related to pegmatite

intrusions (e.g. Harris *et al.,* 1995), even though some of the main ore shoots such as the PC and MMR shoots are known to have been intruded and displaced by late pegmatite bodies (Voges, 1986; Harris *et al.,* 1995).

The most detailed information on geological controls on mineralisation is contained in exploration reports compiled by Anglovaal in the late 1980's and early 1990's (Marchini, 1987; Tomkinson, 1989; Voges, 1989). These reports make mention of the ribbon-like, irregular nature of the ore shoots along the Consort Bar, and suggest this geometry reflects a control by later cross-cutting faults, similar to what has been described in the Sheba-Fairview area (e.g. Dirks *et al.*, 2009). These faults are thought to have introduced the fluids resulting in Arsenopyrite-Pyrrhotite alteration and gold mineralisation as well as retrograde quartz-biotite-chlorite alteration. The controlling faults such as the Ivaura and MMR Faults (Fig. 2) have been described for the MMR and PC shoots (Voges, 1989), but also occur along the orebody near No. 3 and No. 6 Shafts (Marchini, 1987) and in the Witkoppies Quarry where they overprint mylonitised pegmatite zones (Tomkinson, 1987). The MMR Fault is reported to shallow and split into a series of listric fault segments, where it transects the Consort Bar possibly resulting in dilation and ingress of mineralising fluids along the intersection of the faults and the Consort Bar (Voges, 1989; Tomkinson, 1989).

The best estimate for the age of gold mineralisation in the region comes from a quartz porphyry dyke in Fairview Mine dated at 3126±21 Ma (U-Pb, zircon fractions, TIMS; de Ronde *et al.*, 1991). Rutile dated at 3084±18 Ma from the same quartz porphyry (de Ronde *et al.*, 1991) was linked to hydrothermal alteration thought to have resulted in gold mineralisation. Harris *et al*. (1993) reported a poorly constrained Rb-Sr date of 3040±84Ma for a pegmatite that cross-cuts the mineralisation at NCGM, providing a minimum age estimate for the gold.

New details about structural settings of the New Consort Gold Mine

A summary of the regional deformation events in the BGB as documented by de Ronde and de Wit (1994) is presented in Table 1. Additional detailed deformation schemes relevant to the Sheba and NCGM areas have been included in Table 1 from the

work of Viljoen (1964), Anhaeusser (1976) and Dirks *et al.* (2009). In the following section, we present an updated and revised deformation scheme for the NCGM area, based on data collected in this study, which we will use as a framework to explain the geometries that host gold mineralisation around NCGM. To differentiate the new deformation scheme from earlier deformation schemes, we have added 'NC' as a subscript to each of the deformation events described below.

D_{1NC}: pre-Moodies upright folding and thrusting

D_{1NC} structures include tight isoclinal, upright to inclined folds that are restricted to rocks of the Onverwacht and Fig Tree Groups and that are associated with an axial planar fabric which forms a penetrative, S_{1NC}, cleavage throughout the NCGM area. The Consort Bar formed during this event, and probably originated during M_{1NC} peak-metamorphism as a silica enrichment zone along the contact of ultramafic Onverwacht schist and silicic Fig Tree Group metasediment (Schouwstra and De Villiers, 1988). Around NCGM, several tight D_{1NC} antiforms and synforms can be traced (Fig. 3) that are the equivalent of folds such as the Zwartkoppies antiform in the Sheba area (Dirks *et al.*, 2009). An antiformal hinge zone defined by an 80 m wide band of Onverwacht Group schist within Fig Tree rocks, occurs to the south of NCGM (Fig. 3), and is separated from the Consort Bar to the NW by a 100m scale synform positioned in Fig Tree Group schist, which can be traced using changes in the S_0-S_{1NC} bedding-cleavage relationships (Fig.4a). These S_0-S_{1NC} relationships in Fig Tree Group schist vary repeatedly at 10m scales (e.g. GR 307514-7161018) illustrating the presence of isoclinal vergence folds along the larger scale tight folds (Fig. 3). The D_{1NC} antiform of Onverwacht Group rocks within Fig Tree Schist merges with the main body of Onverwacht Group rocks north of the Blue Jacket fault, i.e. E and NE of the mine (Fig. 3) indicating that the fold hinge of the D_{1NC} synform in Fig Tree Schist plunges in a SW direction.

D_{1NC} folds are near-isoclinal and the regional S_{1NC} fabric is generally near parallel to the compositional layering S_0. The orientation of S_{1NC} varies greatly as a result of later folding. S_{1NC} is defined by orientated tremolite, serpentine and mica grains in the

greenstones and by a micaeous schistocity in the greywacke and shale units of the Fig Tree Group.

D_{1NC} is the equivalent of the regional D_2 proposed by de Ronde and de Wit (1994) and D_1 proposed by Dirks *et al*. (2009) (Table 1). The event has been linked to large-scale thrusting between 3.26-3.22 Ga (de Ronde and de Wit, 1994) during the principal accretionary stages of the BGB.

D_{2NC}: Post-Moodies upright folding and thrusting

D_{1NC} folding and metamorphism of the Onverwacht and Fig Tree group rocks was followed by uplift and erosion and then deposition of the Schoongezicht Formation (3225 Ma) and Moodies Group rocks above an angular unconformity (Lowe and Byerly, 1999; Dirks *et al.*, 2009) that is well exposed W and S of NCGM. Once deposited, the Schoongezicht Formation and Moodies Group rocks were compressed during D_{2NC} in a series of upright synforms, of which the Eureka synform to the south of NCGM is the best example (Fig. 1). Older D_{1NC} structures were presumably tightened in the process (Lowe *et al.*, 1999; Dirks *et al.*, 2009). In the NCGM area, D_{2NC} folds are best preserved in synformal inliers as seen along a well-exposed river section of the Noordkaap River west of the NCGM (GR 305460-7161250) and along road and rail sections N of Woodstock Mine (GR 308140-7159150) (Fig. 1).

Along the Noordkaap River folded Schoongezicht Formation and Moodies Group rocks unconformably overlie strongly foliated serpentinite-talc schist of the Onverwacht Group to the W, NW and NE of the synform, and metapelitic schist of the Fig Tree Group to the SE. Agglomerate of the Schoongezicht Formation marks the base of the synclinal sequence, and grades into cross-bedded conglomerate and quartzite in the core of the fold. The units define a strongly asymmetric, upright synclinal synform, 290 m in width, with a 180 m thick E-limb and a strongly attenuated, 40m thick W limb. Flattened pebbles in the agglomerate and conglomerate define an S_{2NC} fabric and an L_{2NC} stretching lineation. S_{2NC} parallels the axial plane of the syncline and trends N to NNW, dipping steeply to the E or W (Figs. 2, 3). S_{2NC} parallels the penetrative S_{1NC} fabric in underlying

Fig Tree Schist suggesting D_{1NC} and D_{2NC} deformation was progressive and coaxial (see also Lowe *et al.*, 1999, and Dirks *et al.*, 2009).

D_{2NC} folds correlate with the large Eureka and Lily Synclines described south of NCGM (Ramsay, 1963; Anhaeusser, 1976; Dirks *et al.*, 2009), and similar large-scale synforms in Moodies Group rocks elsewhere in the BGB (e.g. Lowe *et al*., 1999). The folds formed during the latter stages of accretion of the BGB (Table 1).

D_{3NC}: development of constrictional shears and folds

D_{3NC} structures resulted from a series of progressive events that include the development of a network of shear zones (Fig. 5), which bound structural domains with diverse structural and metamorphic histories. The shear zones form the skeletal framework of the triple junction structure and divide the area around NCGM in separate structural domains (Fig. 5), each characterised by slightly different deformational, metamorphic and exhumation histories (e.g. Dziggel *et al.*, 2007). Movement on the shear zones has been linked to the rise of the Nelspruit Batholith (Viljoen, 1964; Dziggel *et al.*, 2006) imposing a constrictional environment on the area. Complex constrictional folds developed in between the principle shear zones, and in some domains early D_{3NC} shear zones were progressively folded as illustrated by the mylonites of the Consort Bar (Fig. 5). D_{3NC} events, transposed, refolded and tightened the D_{1NC} and D_{2NC} structures and fabrics, and formed concomitant with the large refold of the Eureka syncline S of NCGM (Table 1; Anhaeusser, 1976).

The earliest D_{3aNC} events in the triple junction area involved mylonitisation along a network of shear zones that include the Lily, Albion, Woodstock and Kaap River Faults (Fig. 5), as well as the mylonites along the Consort Bar. The shear zones are characterised by mylonite (Fig. 4b) and ultramylonite (Fig. 4c) with extensive silicification, which in many places takes the form of laminated chert (e.g. Hofmann *et al.,* 2003). Where the shear zones transect ultramafic units, carbonate and fuchsite are common constituents, and mineral rodding, quartz stretching lineations and oriented amphibole growth defines an intense S_{3aNC}-L_{3aNC} fabric. S-C and shear band fabrics are common (Fig. 4b), as are intrafolial folds, which in places assume sheath-like geometries

with fold axes parallel to L_{3aNC}. Shearing along the Consort Bar coincided with the emplacement of an early generation of pegmatite veins along the shear zone. The pegmatites are mylonitised and show quartz and K-feldspar ribbon grains enveloping mantled feldspar porphyroclasts (Fig. 4b), many preserving monoclinic asymmetries.

Figure 5 shows the dominant orientation of L_{3aNC} and shear sense on the main D_{3aNC} shear zones around NCGM. The steeply S to SW dipping Albion, Woodstock and Kaap River Faults all preserve a steeply SW plunging L_{3aNC} lineation, and a SW-up, reverse sense of movement (Fig. 5). The movement sense on the Consort Bar is more complex due to later folding, which affected the orientation of S_{3aNC} and L_{3aNC} (Fig. 6). As the Consort Bar mylonite is traced around the complex folds near NCGM, S_{3aNC} and L_{3aNC} orientations vary (Fig. 6), e.g. east of the MMR ore shoot, L_{3aNC} plunges SE and the shear sense is normal sinistral, and SW of the MMR shoot, L_{3aNC} plunges NW on a moderately W to SW dipping mylonite surface, recording a NW-up, thrust sense of movement. In spite of this complexity, the movement sense consistently indicates that the younger hanging wall units of the Fig Tree Group moved down, relative to the older Onverwacht Group units. This movement sense has been linked to a sharp metamorphic gradient across the fault with Onverwacht Group rocks preserving higher-grade P-T assemblages (e.g. Dziggel *et al.*, 2006).

The structural domain north of the Kaap River Fault, i.e. the area in the immediate vicinity of the NCGM, experienced complex folding during D_{3bNC} and D_{3cNC} events as illustrated by the contorted nature of the Consort Bar. The Consort Bar is folded to produce a generally SE plunging synclinorium composed of several 600m-scale fold structures referred to in the mine from NE to SW as the "Top Section Syncline" the "No. 7 Shaft Anticline", and the "No. 3 Shaft Syncline" (Fig. 3) (Voges, 1986), each associated with several ore bodies (Viljoen, 1964; Voges, 1986; Ward, 1999).

By systematically mapping the orientation of L_{3aNC} and S_{3aNC} along the Consort Bar it can be demonstrated that the synclinorium is not a single fold structure, but instead represents an interference fold pattern of D_{3bNC} and D_{3cNC} folds defining a type 2, dome-crescent-mushroom fold interference pattern (e.g Thiessen, 1986; Ramsay and Huber, 1987). The interference pattern can be illustrated by the domainal nature of D_{3aNC} fabric elements on the different limbs of D_{3bNC} folds, as they bend around the younger D_{3cNC}

structure. Each of the four D_{3bNC} fold limb domains preserves characteristic orientations of older fabric elements such as S_0, S_{3aNC}, and L_{3aNC} (Fig. 6), which can be used to reconstruct the orientation of S_{3bNC} and S_{3cNC} and the regional plunge of the D_{3bNC} and D_{3cNC} folds (F_{3bNC} and F_{3cNC}) (Fig. 6).

D_{3bNC} folds consist of asymmetric, NW-verging, upright, closed folds with a moderately SE dipping fold axial plane, and probably near horizontal fold axis. At least one, 600m-scale synform-antiform pair can be defined (Fig. 6) with smaller scale, vergence folds occurring on their limbs. D_{3bNC} folds were refolded by a single NW trending, steeply reclined closed, D_{3cNC} antiform with a steeply SW dipping fold axial plane and a SE plunging fold axes (Fig. 6).

A good example of a D_{3bNC} fold in outcrop is the reclined, SW plunging synclinal, vertical fold exposed along the road section south of the MMR shaft (GR307379-7162532) where the core of what is referred to as the "Top Section Syncline" is well exposed. The W limb of this structure dips moderately W to SW, whilst the E limb dips moderately S to define a moderately SW plunging fold axes (F_{3bNC} = 225/40; Fig. 6), and a SW dipping fold axial plane (S_{3bNC} = 228/41; Fig. 6).

The core of the D_{3cNC} fold occurs to the SE of Betty's Quarry, where outcrops in the Schoongezicht Formation preserve complex fold interference patterns (e.g. GR 308670-7160500). D_{3cNC} fold axes plunge either to the NW or the SE and vary in orientation depending on the orientation of D_{3bNC} fold limbs, which they overprint (Fig. 7a). A SE plunge is dominant (Fig. 6) reflecting the asymmetric NW verging nature of the underlying D_{3bNC} folds, consistent with general stratigraphic younging to the SE. Excellent examples of D_{3cNC} folds and associated fabrics in outcrop occur in rocks of the Schoongezicht Formation and conglomerate of the Moodies Group S and E of No. 7 shaft (e.g. GR 307875-7160234). D_{3cNc} folds are open, concentric folds associated with a weakly developed axial planar fabric. In conglomerate of the Moodies Group at GR 307875-7160201, pebbles have been flattened (Fig. 4d) under plane strain conditions to define a NW trending, steeply W-dipping axial planar fabric and a moderately SE plunging stretching lineation (Fig. 7b) that parallels the fold axes of 1-5 m scale folds.

D_{4NC} : late kink-folding and normal faulting

D_{4NC} structures comprise shallowly dipping sets of conjugate kink folds that can be linked to a network of brittle-ductile shear zones with a normal sense of movement (Anhaeusser, 1976; Dirks *et al.*, 2009). D_{4NC} kink folds are typically about 2 to 4 meters in size and mainly trend SE and E, dipping shallowly SW and S respectively. They occur as localised structures with crenulation cleavage and extensional brittle-ductile shear zones cutting across the cores of the kinks along the traces of axial planes. Fully developed conjugate pairs (e.g. GR 307869-7163737) with well-defined conjugate normal shears are common. Good examples of kink folds can be found in the Mine Manager Quarry (GR 308230-7159033) and along the railway siding (GR 307970-7159190) north of Woodstock Mine. In places (e.g. NW of MMR), the axial planes of kink folds are silicified and invaded by quartz veins and pegmatite units.

The most prominent D_{4NC} structures are brittle-ductile extensional shear zones, commonly associated with quartz veining, sericitisation, silicification and biotite-chlorite alteration as well as sulphide growth. D_{4NC} shear zones are always present in the old gold workings, and stoping commonly occurs along the shears suggesting a close association with gold mineralisation (Figs. 4e, f). The most prominent of these have been named (e.g. the MMR and Ivaura Faults; Fig. 2).

Good examples of mined, mineralised brittle-ductile shears can be found in the Witkoppies, Betty and Mine Manager Quarries (Fig. 2), and in large pits found in both Albion and Woodstock gold mines (Fig. 1). The shears typically occur as 25-30 cm wide zones in which a strong foliation has developed defined by schistose micaceous zones that are sulphidised in places. This foliation is truncated by discrete, 5-7 mm-wide fracture planes (Fig. 4g) commonly associated with slickensided surfaces with slickenfibre lineations defined by quartz or calcite with steps indicative of a mostly normal movement sense (similar to that recorded in the MRC Section of Sheba mine, Fig. 4h). Several generations of quartz veining including early black, cherty veins and later milky veins, with associated carbonate and chlorite growth are common, as is sulphidisation and silicification affecting the wall rock for several meters on either side of

individual shear zones, with wider alteration zones occurring in areas of complex intersections between two or more shear zones.

On the scale of individual workings such as the 100x100m Witkoppies quarry, a number of D_{4NC} shear zones can be traced that display a wide variety of orientations (Fig. 8) and complex cross cutting relationships, although almost all of these shears accommodated a normal sense of movement component. Individual shears in the Witkoppies Quarry can be traced for tens of metres and have moderate dips (30-60 degrees) to the SE, S or SW, and slickenline orientations that plunge predominantly at low to medium angles to the SSE-SE (Fig. 8). Individual faults occur in en echelon and cross cutting arrays across the pit to define two roughly NNW and ENE trending fault corridors, which also define the shape of the open pit and distribution of surrounding adits.

The fault pattern in the well-exposed Wikoppies Quarry is representative for other workings in the NCGM area, such as Mine Manager Quarry (Fig. 9). Although near vertical NNW-trending strike-slip faults are observed in places, steeply S-dipping and ENE trending normal faults are dominant especially in pits along the MMR and PC shoots (Figs. 8). By mapping individual faults in surface workings across the hills, a larger scale pattern of mineralised brittle-ductile fractures arises (Fig. 10), including a 120 m wide central NNW trending corridor of fractures between the Ivaura workings in the NNW via the Wikoppies Quarry and Hard Cash to the workings around No. 7 shaft in the SSE (Fig. 10). This corridor is transected by several WNW and ENE trending fracture corridors including one along the MMR workings in the north, one along the Bluejackets, Mine Manager, Betty's and PC workings in the centre, and one along the No. 3-No. 6 workings to the SW of the NCGM (Fig. 10). In each of these corridors, individual brittle-ductile shear zones can be traced for up to 100-140 m along which pits, shafts and trenches have been developed (Fig. 10). As a mineralised fracture terminates, a new one starts up, commonly in a slightly displaced, but overlapping en-echelon manner, whilst cross fractures connect both shear zone strands. In the northern part of the NCGM, The WNW trending corridor along the MMR workings is 200-250 m in width, and contains NW-trending, mineralised fractures up to 250 m in strike length, and shorter SW

trending cross fractures. The mineralised corridor dips moderately SSW to coincide with the orientation of projected ore shoots at depth as indicated by Voges (1989; Fig. 10).

Extensional brittle-ductile shear zones in relation to gold mineralisation also characterises the workings of nearby Albion, Woodstock and Clutha Mines (Fig. 11), and have been described from the workings in the Sheba-Fairview mine area (Dirks *et al.*, 2009). In the Woodstock Mine, workings occur along an ENE trending corridor that extends for a kilometre and consists of several, E-trending fractures arranged in en echelon fashion and cut by SE-trending cross fractures (Figs. 8, 11).

Gold-bearing shear zones are associated with silica alteration, involving quartz veining, and the development of larger silica alteration haloes. A good example of this occurs in Woodstock Mine, where a complex, 10-30m wide stock work zone of milky quartz veins accompanied by pervasive silica alteration forms a massive chert-like unit immediately adjacent to the sulphidic ore zone. Large (600 x 300m) areas affected by pervasive silica alteration also characterise the area between PC and 7 Shafts (Fig. 10). These alteration zones are found in the hanging wall of mineralised horizons and form topographically pronounced features (GR 307870-7161250) characterized by altered host rocks, locally invaded by stockworks of thin chert veinlets (see also Dirks *et al.,* 2009).

D_{5NC}: late stage shear zones

D_{5NC} structures include brittle-ductile shear zones that accommodated a reverse sense of movement and crosscut the extensional shears associated with gold mineralisation. D_{5NC} reverse shears have been observed in several gold workings with good examples in the Albion Mine, but their larger scale geometry is unclear. They are indicative of reactivation of gold-bearing shears as thrusts, and are associated with carbonate and silica alteration including late-staged quartz veining.

Palaeo-stress Analyses

Field observations indicate that gold mineralisation in the NCGM is spatially associated with D_{4NC} retrograde, extensional brittle-ductile shear zones that cross-cut a

complex sequence of older, D_{1NC}-D_{3NC} ductile structures which impart a complex geometry on the area. To investigate the timing of mineralisation further and put constraints on the tectonic regime, a kinematic analysis of the D_{4NC} fractures was undertaken across the NCGM area and nearby mines.

Kinematic data from faults including the orientation of the fault plane, the slip direction visible as slickenlines, striations or gouge marks, and the sense of movement was used to reconstruct palaeo-stress fields (*e.g.* Angelier and Mechler, 1977). Stress inversion techniques rely on the assumption that the slip direction coincides with the resolved shear stress on the fault plane, and that the set of faults used in the analysis, were active in response to that stress field. Fault-slip data can be inverted to a reduced moment tensor with information on the direction of the principle stress axes and their relative (arbitrary) magnitude expressed as a stress ratio (Angelier, 1994; Delvaux and Sperner, 2003). This reduced stress tensor can be calculated using the P and T axes that bisect the fault plane and an auxiliary plane perpendicular to the fault, by using least-square minimization techniques of direction cosines (*e.g.* Marrett and Allmendinger, 1990) or iterative methods that test a variety of possible tensor solutions (*e.g.* Etchecopar *et al.*, 1981). Stress axes can also be determined graphically using the right dihedron method (Lisle, 1987; Delvaux and Sperner, 2003), which constrains the orientation of principle stress axes by determining the area of maximum overlap of compressional and extensional quadrants for a suite of faults.

In analyzing the fault-slip data from gold workings around the triple junction we have used the 2009 Windows version of the programme TENSOR (Delvaux, 1993; 2009), which uses an expanded right dihedron method described in Delvaux and Sperner (2003). Results have been compared with a linked Bingham distribution tensor calculated with the programme FaultKin (Allmendinger, 2001) following methods described by Marrett and Allmendinger (1990) and Cladouhos and Allmendinger (1993).

The TENSOR programme follows the basic numerical approach outlined by Angelier (1994). Principle stress axes (σ_1, σ_2 and σ_3) and the ratio of principle stress differences ($R = (\sigma_2-\sigma_3)/\sigma_1-\sigma_3)$) are determined using an improved version of the method of Angelier and Mechler (1977), optimized by minimizing deviation angles (α) between observed and predicted slip vectors on fault planes, and by maximizing the shear stress

magnitude (σt) on fault planes. This is done using an iterative procedure that involves successive rotations on σ_1, σ_2 and σ_3 axes until an optimal fit is found (see Delvaux and Sperner, 2003). Misfits in the dataset can be identified and excluded in an interactive manner. A quality assessment for the data is provided following quality ranking schemes developed in the World Stress Map Project (*e.g.* Sperner *et al.*, 2003). This scheme combines assessments of the type and quality of data used, with quantitative assessments of the size of the data set, the distribution of slip and fault plane data and the average slip deviation between the observed and predicted slip vectors, to provide a quality ranking (QRw) ranging from A (best) to E (worst) (Delvaux and Sperner, 2003). The type of stress regime can be expressed as a stress ratio R, which varies from constrictional (R=1 with $\sigma_1 = \sigma_2$) via plane (R =0.5 with $\sigma_1>\sigma_2>\sigma_3$) to flattening stress (R = 0 with $\sigma_2 = \sigma_3$), and varies with the orientation of the principle stress axes. Delvaux and Sperner (2003) define a parameter R′ to express the stress regime numerically as a number between 0 and 3 with R′ = R when σ_1 is sub-vertical (*i.e.* plunging steeper than 45° representing an extensional stress regime), R′ = 2 - R when σ_2 is sub-vertical (strike-slip stress regime) and R′ = 2 + R when σ_3 is sub-vertical (compressional stress regime). The parameters R and R′ will be referred to with reference to gold mineralization in the NCGM area as well. The programme output is a diagram displaying the fault-slip data, a histogram of α values, a diagram showing the horizontal maximum and horizontal minimum stress axes, the orientation of σ_1, σ_2 and σ_3, the R value and a quality ranking (Fig. 8).

The FaultKin programme (Allmendinger, 2001) uses the distribution of P and T axes for a suit of faults (Angelier and Mechler, 1977) to calculate a Bingham axial distribution based on a least squares minimization technique for direction cosines. The auxiliary plane has been calculated assuming P is at 45º from the fault. The eigenvectors for the calculated Bingham axial distribution provide average orientations for the maximum, minimum and intermediate concentration direction of the P and T axes, and the eigenvalues provide a measure of the relative concentration of P and T axes. These eigenvalues vary between -0.5 and +0.5, with maximum values reached when P and T axes are perfectly concentrated. Variations in the eigenvalues provide a measure of the distribution of the P and T axes. The FaultKin programme output is a plot of linked

Bingham axes with eigenvalues and a related fault plane solution diagram displaying P and T quadrants in a manner similar to earthquake focal mechanisms (Table 2).

Although stress analysis from fault slip data is widely applied, debate continues whether the obtained solutions represent a stress field or provide a measure of strain and strain rate (*e.g.* Molnar, 1983, Twiss and Unruh, 1998). Marrett and Allmendinger (1990) and Allmendinger (2001), using FaultKin, prefer to interpret the fault plane solutions as an indicator of strain rather than stress, whilst the output of TENSOR is presented in terms of stress regimes (Delvaux and Sperner, 2003; Sperner *et al.*, 2003). In spite of the difference in approach, the results of the FaultKin programme can be directly compared with the TENSOR programme (e.g. Dirks *et al.*, 2009).

Because we use the same datasets to generate a linked Bigham fault plane solution through FaultKin and an improved right dihedron solution using an iterative approach in TENSOR, we will interpret all results as an indication of the palaeo-stress field. In doing this, we are aware that faults, once formed, can interact in complex ways in response to an imposed stress-field due to scale-dependent strain partitioning, complex fault interactions, block rotations, and inhomogeneities in the rock mass (*e.g.* Twiss and Unruh, 1998). In spite of such limitations, the palaeo-stress analysis technique has been successfully applied in a wide variety of tectonic settings (*e.g.* Sperner *et al.*, 2003), and we believe that it does provide valuable insights in the tectonic controls on gold mineralization in the NCGM and surrounding areas (see also Dirks *et al.,* 2009).

Selection of faults for kinematic analysis

In selecting faults for analyses we have focused on surface workings where stoping occurs along brittle-ductile shear zones that display slickensided surfaces and sulphide alteration (Figs. 4e, f, g, h). Support pillars left behinds in stopes (*e.g.* Figs. 4e, f) provide excellent sites to observe the shears associated with the highest grade of mineralization and ensure that our data set can be linked to mineralization. Working on the assumption that gold mineralization occurred in response to a single late-tectonic phase in the evolution of the greenstone belt (*e.g.* de Ronde *et al.*, 1991; de Ronde and de Wit, 1994) this approach will ensure a relatively homogeneous input data set.

A common problem encountered in selecting data is that some mineralized fractures contain more than one lineation; commonly one steep- and one shallow-pitching lineation. It is generally not clear whether such overprinting lineations reflect separate events (e.g. D_{4NC} and D_{5NC} events) or form as a result of slip partitioning in a continuous D_{4NC} event. To prevent subjective bias, both sets of lineations have been included in the data sets.

Misfits in the collected datasets may have resulted from observational errors or the mixing of unrelated data points. They can also be due to non-uniform stress fields as a result of fault interactions, anisotropies in the rock mass, block rotations or slip partitioning. In our analyses using TENSOR we have kept manual cleaning of the data sets to a minimum considering that much of the pre-selection of the data was done in the field by only picking mineralised fault planes. In calculating a Bingham tensor solution using FaultKin all data points were included.

Data of several pits occurring along the same mineralisation corridor (Fig. 10) have been grouped together to calculate an average solution for the palaeo-stress field. Because individual pits are commonly developed on a single fracture, or group of parallel fractures, measurements from such pits may place an undue emphasis on one particular fracture orientation (and corresponding local palaeo-stress field). By combining pits within a mineralisation corridor a wider variety of fracture orientations is included, and partitioning effects, or observational bias due to strain partitioning along any one fracture is reduced (Fig. 10).

Thus, the data sets for the NCGM area have been grouped into the NNW, WNW and ENE trending corridors described above (Fig. 10). The data from individual corridors is compared with the total data set from NCGM and with data sets obtained from nearby workings at the Albion Mine, the Clutha Mine and the Woodstock Mine, to allow an assessment of the regional nature of the calculated stress field.

Results of kinematic analyses

The results of kinematic analyses from fracture planes in gold workings in the NCGM are presented in Figure 10 and summarised in Table 2.

Bingham tensor solutions in FaultKin

The results for the MMR workings along the WNW trending corridor display a pure extensional stress regime (R = 0.51, R' = 0.51) with σ_1 being near-vertical and σ_3 being horizontal and orientated at 136º/10º. The results for the workings along the ENE trending corridor between Mine managers Quarry and Witkoppies quarry are almost identical with a pure extensional stress regime (R = 0.41, R' = 0.41) and σ_1 near-vertical and σ_3 orientated at 149º/04º. Results for the NNW trending corridor also display a pure extensional stress regime (R = 0.60, R' = 0.60) with σ_1 remaining near-vertical and σ_3 remaining horizontal and orientated at 330º/06º (Fig. 10, Table 2a) .

The combined result for the workings in the NCGM shows a near vertical σ_1 orientation, with σ_3 at 148º/04º and σ_2 at 238º/17º (Table 2a). An indication for the stress regime as calculated from the eigenvalues suggests a pure extensional setting (Table 2a). Results for the Albion, Clutha and Woodstock mines are similar (Table 2a).

Optimized dihedron method in TENSOR

The results for the MMR workings along the WNW trending corridor display a pure extensional stress regime (R = 0.49, R' = 0.49) with σ1 being near-vertical and σ_3 being horizontal and orientated at 109º/01º (Table 2b). The results for the workings along the ENE trending corridor between Mine Managers and Witkoppies Quarries show a dominant radial extensional stress regime (R = 0.16, R' = 0.16) with σ_1 near-vertical and σ_3 orientated at 342º/01º (table 2b). Results for the NNW trending corridor display a pure extensional stress regime (R = 0.54, R' = 0.54) with σ_1 remaining near-vertical and σ_3 horizontal and orientated at 327º/09º (Table 2b).

The combined result for the workings in the NCGM shows a near vertical σ_1 orientation, with σ_3 at 318º/06º and σ_2 at 228º/03º (Table 2b). An indication for the stress regime as calculated from the eigenvalues suggests a pure extensional setting (Table 2b). Results for the Clutha, Albion and Woodstock mines are similar (Table 2b).

Discussion

In this study, five deformation events (D_{1NC} – D_{5NC}) have been described from the NCGM area. D_{1NC} - D_{3NC} events involve progressive shearing and folding events linked to the accretionary history of the greenstone belt (D_{1NC} and D_{2NC}), and subsequent doming of surrounding batholiths (D_{3NC}). D_{4NC} structures comprise a network of extensional brittle-ductile shear zones and associated kink bands and crenulation folds that formed concomitant with gold mineralisation. D_{5NC} structures represent late reverse faults.

D_{1NC} is restricted to Onverwacht and Fig Tree Group rocks and produced a penetrative cleavage axial planar to a series of tight antifoms and synforms. The contact between the Fig Tree and Onverwacht Group rocks was strongly sheared and silicified to result in a discrete unit called the Consort Bar. D_{1NC} events can be linked to D2 events of de Ronde and de Wit (1994) and Lowe et al. (1999), interpreted to have occurred between 3260 – 3225 Ma.

An angular unconformity separates the Fig Tree and Onverwacht group rocks from the overlying volcaniclastic units of the Schoongezicht Formation and Moodies Group (Dirks et al., 2009). Thus Fig Tree and Onverwacht Group rocks were uplifted and eroded prior to deposition of the volcaniclastics. Subsequent D_{2NC} folding of the rocks in large synformal structures, that trend parallel to the D_{1NC} folds suggest that these events are part of a progressive compressional regime during the later stages of accretion of the BGB (e.g. Lowe *et al*.,1999) .

D_{3NC} structures resulted from a series of progressive events that include the development of a network of shear zones, which divide the area around NCGM in separate structural domains, each characterised by slightly different deformational, metamorphic and exhumation histories (e.g. Dziggel *et al.*, 2006, 2007). Movement on the shear zones has been linked to the rise of the Nelspruit Batholith (Viljoen, 1964; Dziggel *et al.*, 2006) imposing a constrictional environment on the area. Around NCGM, complex fold interferences developed in between the principle shear zones. Early D_{3aNC} shear zones visible as mylonites along the Consort Bar were folded during D_{3bNC} and

D_{3cNC} events. This happened concomitant with the large refold of the Eureka Syncline S of NCGM (Table 1; Anhaeusser, 1976).

D_{3bNC} folds consist of asymmetric, NW-verging, upright, closed folds with a moderately SE dipping fold axial plane, and probably near horizontal fold axis. D_{3bNC} folds were refolded by a single NW trending, steeply reclined closed, D_{3cNC} antiform with a steeply SW dipping fold axial plane and a SE plunging fold axes. This refolded-fold pattern is responsible for the complex distribution of the Consort Bar both on surface and underground (Voges, 1986). Given that the Consort Bar constitutes an ideal trapping zone for subsequent god mineralisation, the complex distribution of the Consort Bar imposed by the refolded-fold pattern has resulted in equally complex distributions of underground ore zones. Although common trends of ore zones are known from mined areas, fold interference-pattern make down dip projections of ore shoots extremely difficult.

The complex fold interference pattern has resulted in mis-interpretations of the local geology. A good example is the Shires Shear Zone (SSZ), which has been described in mine reports (Tomkinson, 1989) and has been referred to as an important gold-bearing structure (e.g. Harris *et al.,* 1995; Dziggel *et al.*, 2007; Otto *et al.*, 2008). The SSZ has been described underground from an area that coincides with the No.7 Antiform, between Witkoppies Quarry and No. 6 shaft (Figs. 2 and 3). This package of isoclinal D_{3bNC} folds, repeatedly fold and duplicate D_{3aNC} mylonite along the Consort Bar. Underground drives crossing these folds, display a wide zone of D_{3aNC} mylonite as the Consort Bar is repeatedly crossed, creating the impression of a complex wide shear zone (Tomkinson, 1989; Harris *et al.*, 1995). On surface no evidence can be found for the SSZ.

The Bluejackets Fault is another example of an important structure that has been misinterpreted as a single, late, normal fault that post-dates mineralisation (e.g. Voges, 1986). The presence of mylonitised and non-mylonitised pegmatites, and mylonitic chert with clear $S3_{aNC}$ and $L3_{aNC}$ fabrics found along the Bluejackets structure indicate that the fault zone is a continuation of the Consort Bar, be it strongly attenuated, which presumably occurred during $D_{3a\text{-}bNC}$ shearing and folding events. This ductile structure was overprinted by en-echelon, brittle-ductile, E-W trending D_{4NC} normal faults, many of which show evidence of low-grade gold mineralisation as demonstrated by the presence of surface workings.

Our results show that gold mineralisation can be linked to a network of extensional brittle-ductile shear zones that cross-cut, the complex refolded fold patterns in the NCGM. By mapping individual faults in surface workings across the hills around NCGM, a larger scale pattern of D_{4NC} brittle-ductile fractures zones or deformation corridors can be constructed. The D_4 fracture corridors include a 120 m wide central NNW trending corridor of fractures between the Ivaura workings in the NNW and No. 7 shaft in the SSE. A WNW trending corridors along the MMR workings and two ENE trending corridors, one between Witkoppies, and Mine Managers quarries, and one between the No. 3-No. 6 workings to the SW of the NCGM. In each of these corridors, complex fracture patterns define apparent Riedel, anti-Riedel and P-shear arrays, all preserving a component of normal movement, associated with abundant quartz veining and extensive silicification, carbonatisation and sulphide growth.

Gold workings occur along the network of D_{4NC} fracture corridors within the general area characterised by pervasive silica alteration. High-grade ore-shoots, including PC, Ivaura, No. 3 and No. 7 shoots have formed where D_{4NC} extensional brittle-ductile shear zones crosscut the complexly folded, laminated cherts of the Consort Bar, or the silicified mafic-ultramafic Onverwacht Group units in its immediate footwall, which appear to trace the location of a D_{1NC} fold hinge. Such silicified cross-cutting fracture zones near the Consort Bar are known to contain abundant, non orientated arsenopyrite grains indicative of good gold (Marchini, 1987). These observations indicate that the highly silicified hinge zones of D_{1NC} isoclinal folds as well as the silicified and mylonitised contact zone between the Fig Tree and Moodies Groups constitute the best trapping structures for gold bearing fluids introduced during D_{4NC} along networks of brittle-ductile fracture corridors.

The introduction of the auriferous fluids may be linked to the magmatic fluids related to pegmatite emplacement as suggested by Harris *et al.* (1995), which themselves have been linked to emplacement and doming of the Nelspruit Batholith (Harris, 1992), which would have presumably occurred around 3106 Ma (Kamo and Davis, 1994). Pegmatites, however, are common along the northern margin of the BGB, and only around NCGM are they closely associated with gold mineralisation. The alternative explanation for the introduction of auriferous fluids is that it was related to a magmatic

event that post-dated emplacement of the Nelspruit Batholith possibly around 3084+/-18 Ma (de Ronde *et al.*, 1992) and involving the emplacement of porphyry dykes in the area (Dirks *et al.,* 2009).

Palaeo-stress analysis for D_{4NC} fault planes in the NCGM area, using Bingham fault plane solutions (Figs. 10 and 11) and optimized dihedron methods (Figs. 10 and 11) from the NCGM show consistent results with σ_1 being near vertical and σ_3 horizontal directed along a NW-SE axis. Results for the NCGM area are near identical to results from Clutha, Woodstock, Albion and those reported for the Sheba area by Dirks *et al*. (2009). This suggests that all gold-bearing structures formed within the same extensional tectonic setting, and that the extensional stress field was probably of regional significance. Judging from the dominance of NW or SE directed slip directions on the multitude of D_{4NC} fault plane directions, a pure extensional stress regime is most common as can also be seen from the calculated stress tensor results (Table 2).

The critical structures controlling gold mineralisation are the extensional D_{4NC} fault zones. The distribution of high-grade ore zones is a function of the intersection orientation of the D_{4NC} fault zones with suitable host lithologies, which display a complex distribution pattern as a result of D_{1NC}-D_{3bNC}-D_{3cNC} fold interference patterns. The 3-D distribution of ore zones is therefore discontinuous and complex.

In tectonic terms the extensional D_{4NC} structures overprint all earlier ductile structures that can be linked to the 3260-3225 Ma accretionary stages of the BGB (i.e. D_{1NC}-D_{2NC} events; Table 1) or to events linked to emplacement and doming of the Nelspruit Batholith around 3106 Ma (i.e. D_{3NC} events; Table 1). Mineralisation can therefore be linked to an extensional event that may have developed separately from the accretionary events shaping the craton; i.e. after stabilisation of the craton had occurred. The presence of such an extensional event has been noted before (e.g. de Ronde and de Wits, 1994; Dirks *et al.,* 2009), and explained as extensional collapse of the craton possibly related to the opening of intracratonic basins in which volcanic and sediments of the Dominion Group were deposited shortly before 3074 ± 6 Ma (Armstrong *et al.*, 1991).

It is important to note that the ingress of auriferous fluids could have occurred after accretion and stabilisation of the craton; the later being linked to the widespread emplacement of high-K granites around 3105 Ma (Robb *et al.*, 2006; Dirks and Jelsma, 1999). This indicates that classifying deposits like the NCGM as orogenic is misleading even though the lode-gold deposits are hosted by accretionary greenstone sequences. Instead their tectonic position in time and space is better explained as extensional intracratonic.

Acknowledgements

Our sincere thanks go to Sheba, Fairview and New Consort mines and especially to the geology team: Chris Rippon, Charles Robus and Roelf LeRoux who for many years have allowed us generous access to workings, mine reports, drill core and exploration data. Your support has been fantastic and we hope the results are of use. Financial and in-kind support from Africa Array (PD, GC and RM), The University of the Witwatersrand (GC), New Consort Mine (RM) and the Royal Bafokeng Trust (RM) is kindly acknowledged.

References

Allmendinger, R.W. (2001). FaultKinWin, Version 1.1: a program for analyzing fault slip data for Windows™. (www.geo.cornell.edu/geology/faculty/RWA/programs.html).

Allmendinger, R.W. (2002). StereoWin for Windows. (www.geo.cornell.edu/geology/faculty/RWA/programs.html).

Angelier, J. (1994). Fault slip analysis and palaeostress reconstruction. *In:* Hancock, P.L. (Ed.). *Continental Deformation*. Oxford, Pergamon, Oxford, 101-120.

Angelier, J., and Mechler, P. (1977). Sur une méthode graphique de recherche des contraintes principales également utilisable en tectonique et en séismologie: la méthode des dièdres droits. *Bulletin de la Société Géologique de France*, **7**, 1309-1318.

Anhaeusser, C.R. (1969). *The stratigraphy, structure, and gold mineralization of the*

Jamestown and Sheba Hills Areas of the Barberton Mountain Land. Ph.D.thesis (unpubl), Univ. Witwatersrand, Johannesburg, 332 pp.

Anhaeusser, C.R. (1976). The Geology of the Sheba Hills area of the Barberton Mountain Land, South Africa, with particular reference to the Eureka syncline. *Transactions of the Geological Society of South Africa*, **79**, 253-280.

Armstrong, R.A., Compston, W., Retief, E.A., Williams, I.S. and Welke, H.J. (1991). Zircon ion microprobe studies bearing on the age and evolution of the Witwatersrand triad. *Precambrian Research*, **53**, 243-266.

Brandl, G., Cloete, M. and Anhaeusser, C.R. (2006). Archaean Greenstone Belts. *In:* M.R. Johnson, C.R. Anhaeusser, and R.J. Thomas (Eds.), *The Geology of South Africa*. Geological Society of South Africa-Council for Geoscience, Pretoria, 9-56.

Byerley, G.R., Kröner, A., Lowe, D.R., Todt, W. and Walsh, M.M. (1996). Prolonged magmatism and time constraints for sediment deposition in the early Archaean Barberton greenstone belt: evidence from the Upper Onverwacht and Fig Tree Groups. *Precambrian Research*, **78**, 125-138.

Cladouhos, T.T. and Allmendinger, R.W. (1993). Finite strain and rotation from fault slip data. *Journal of Structural Geology*, **15**, 771-784.

Condie, K.C. (1981). *Archean Greenstone Belts*, Developments in Precambrian Geology 3, Elsevier, 434 pp.

Condie, V.C., Macke, J.E. and Reimer, T.O. (1970). Petrology and geochemistry of early Precambrian graywackes from the Fig Tree Group, South Africa. *Geological Society of America Bulletin*, **81**, 2759-2776.

de Ronde C.E.J., Kamo S., Davis D.W., de Wit M.J. and Spooner E.T.C. (1991). Field, geochemical and U-Pb isotopic constraints from hypabyssal felsic intrusions within the Barberton greenstone belt, South Africa: implications for tectonics and the timing of gold mineralization. *Precambrian Research*, **49**, 261-280.

de Ronde C.E.J., Spooner, E.T.C., de Wit, M.J. and Bray, C.J. (1992). Shear zone related, Au quartz vein deposits in the Barberton greenstone belt, South Africa: field and petrographic characteristics, fluid properties, and light stable isotope geochemistry. *Economic Geology*, **87**, 366-402.

de Ronde E.J. and de Wit M.J. (1994). The tectonic history of the Barberton greenstone belt South Africa: ~490 million years of Archaean crustal evolution. *Tectonics*, **13**, 983-1005.

Delvaux, D. (1993). The TENSOR program for palaeostress reconstruction: examples from the East Africa and Baikal rift zones: *Terra Abstracts, Abstract supplement No. 1 to Terra Nova*, **5**, p. 216.

Delvaux, D. (2009). Windows version of the Tensor program (Win-Tensor). http://users.skynet.be/damien.delvaux/Tensor/tensor-index.html

Delvaux D. and Sperner, B. (2003). New aspects of tectonic stress inversion with reference to the TENSOR programme. *In:* D.A. Nieuwland (Ed.), New insights into structural interpretation and modelling. Geological Society of London, Special Publication, 212, 75-100.

Dirks, P.H.G.M. and Jelsma, H.A. (1998). Horizontal Accretion and Stabilization of the Zimbabwe Craton. *Geology*, **26**, 11-14

Dirks, P.H.G.M., Charlesworth, E.G. and Munyai, M.R. (2009). Cratonic extension and Archaean gold mineralisation in the Sheba-Fairview mine, Barberton Greenstone Belt, South Africa. *South African Journal of Geology*, **112**, 291-316.

Dziggel, A., Knipfer, S., Kisters, A.F.M. and Meyer, F.M. (2006). P-T and structural evolution during exhumation of high-T, medium-P basement rocks in the Barberton Mountain Land, South Africa. *Journal of Metamorphic Geology*, **24**, 535-551.

Dziggel, A., Otto, A., Kisters, AFM and Meyer, F.M. (2007). Tectono-metamorphic controls on Archean gold mineralization in the Barberton greenstone belt, South Africa: An example from the New Consort Gold Mine. *In:* M.J. van Kranendonk, R.H. Smithies and C.B. Vickie (Eds.), *Earth's Oldest Rocks*. Development in Precambrian Geology, **15**, Elsevier, Amsterdam, 699-727.

Etchecopar, A., Vasseur, G. and Daignières, M. (1981). An inverse problem in microtectonics for the determination of stress tensors from fault striation analysis. *Journal of Structural Geology*, **3**, 51-65.

Goldfarb, R.J., D.I. and Gardoll, S. (2001). Orogenic gold and geologic time: a global synthesis. *Ore Geology Reviews*, **18**, 1-75.

Groves, D.I., Goldfarb, R.J., Gebre-Mariam, M., Hagemann, S.G. and Robert, F. (1998). Orogenic gold deposits: a proposed classification in the context of their crustal distribution and relationship to other gold deposit types. *Ore Geology Reviews*, **13**, 7-27.

Harris, P.D. (1992). *The evolution and structural setting of Pegmatites at the New Consort Gold Mines, Barberton Greenstone Belt*. M.Sc. thesis (unpubl.), Univ. Witwatersrand, Johannesburg, 114 pp.

Harris, P.D., Smith , C.B., Hart, R.J. and Robb, L.J. (1993). Sm-Nd and Rb-Sr isotope systematics of rare-element pegmatites from the New Consort Gold Mine, Barberton Mountain Land, South Africa. *Inform. Circ. Econ. Geol. Res. Unit, Univ. Witwatersrand, Johannesburg,* **265**, 20pp.

Harris, P.D., Robb, L.J. and Tomkinson, MJ. (1995). The nature and structural setting of rare-element pegmatites along the northern flank of the Barberton greenstone belt, South Africa. *South African Journal of Geology*, **98**, 82-94.

Hearn, M.G. (1943). *A study of the working properties of the chief gold producer of the Barberton District, Eastern Transvaal.* Ph.D. thesis (unpubl.), Univ. Witwatersrand, Johannesburg, 201 pp.

Hofmann, A. (2005). The geochemistry of sedimentary rocks from the Fig Tree Group, Barberton greenstone belt: Implications for tectonic, hydrothermal and surface processes during mid-Archaean times. *Precambrian Research*,**143**, 23-49.

Hofmann, A., Dirks, P.H.G.M., Jelsma, H.A. and Matura, N. (2003). A tectonic origin for ironstone horizons in the Zimbabwe Craton and their significance for greenstone belt geology. *Journal of the Geological Society of London*, **160**, 83-97.

Kamo S.L. and Davis D.W. (1994). Reassessment of Archaean crustal development in the Barberton Mountain Land, South Africa, based on U-Pb dating. *Tectonics*, **13**, 167-192.

Kröner, A., Hegner, E., Byerley, G.R. and Lowe, D.R. (1992). Possible terrane identification in the early Archaean Barberton Greenstone Belt, South Africa, using single zircon geochemistry. *EOS (Transactions American Geophysical Union)*, **73**, p. 616.

Lisle, R. J. (1987). Principal stress orientations from faults: an additional constraint. *Annales Tectonic*, **1**, 155-158.

Lowe, D.R. (1994). Accretionary history of the Archean Barberton Greenstone Belt (3.55-3.22 Ga), southern Africa. *Geology*, **22**, 1099-1102.

Lowe, D.R. and Byerly, G.R. (1999). Stratigraphy of the west-central part of the Barberton Greenstone Belt, South Africa. *Geological Society of America Special Paper* **329**, Boulder, Colorado, 1-36.

Lowe, D.R. and Byerly, G.R. (2007). An overview of the geology of the Barberton greenstone belt and vicinity: Implications for early crustal development. *In:* M.J. van Kranendonk, R.H. Smithies and C.B. Vickie (Eds.), *Earth's Oldest Rocks*. Development in Precambrian Geology, **15**, Elsevier, Amsterdam, 481- 524.

Lowe, D.R., Byerly, G.R. and Heubeck, C. (1999). Structural divisions and development of the west-central part of the Barberton Greenstone Belt, South Africa. *Geological Society of America Special Paper* **329**, Boulder, Colorado, 37-82.

Marchini, D. (1987) *Controls on gold mineralisation within the 1 Shaft - 3 Shaft area, 3 Shaft Syncline*. Anglovaal Internal Report (unpubl.), ETC/AVE/87/135, 18pp.

Marrett, R. A., and Allmendinger, R.W. (1990). Kinematic analysis of fault-slip data, *Journal of Structural Geology*, **12**, 973-986.

Molnar, P. (1983). Average regional strain due to slip on numerous faults of different orientations. *Journal of Geophysical Research*, **88**, 6430-6432.

Otto, A., Dziggel, A., Kisters, A.F.M. and Meyer, F.M. (2007). The New Consort Gold Mine, Barberton greenstone belt, South Africa: orogenic gold mineralization in a condensed metamorphic profile. *Mineralia Deposita*, **42**, 715-735.

Ramsay, J.G. (1963). Structural investigations in the Barberton Mountain Land, eastern Transvaal. *Transactions of the Geological Society of South Africa*, **66**, 353-401.

Ramsay, J.G. and Huber, M.I. (1987). *The techniques of modern structural geology, Volume 2: Folds and Fractures*. Academic Press, 700pp.

Robb, L.J. (2004). *Introduction to ore-forming processes*. Malden, MA : Blackwell Publication, 373 p.

Robb, L. J., Brandl, G., Anhaeusser, C.R. and Poujol, M. (2006). Archaean Granitoid Intrusions. *In:* M.R. Johnson, C.R. Anhaeusser, and R.J. Thomas (Eds.), The

Geology of South Africa. Geological Society of South Africa-Council for Geoscience, Pretoria, 57-94.

Schouwstra, R.P. and De Villiers, J.P.R. (1988). Gold mineralization and associated wallrock alteration in Main Reef Complex at Sheba mine, South Africa: *Transactions of the Institute of Mining and Metallurgy*, **97B**, 158-170.

Sibson, R. H. (2001). Principles of structural control on permeability and fluid flow in hydrothermal systems. *In:* J.P. Richards and R.M. Tosdal (Eds.), *Structural controls on ore genesis*. Society of Economic Geologists, Boulder, Colorado, Reviews in Economic Geology, **14**, 25-50.

Sibson, R.H. (2004). Controls on maximum fluid overpressure defining conditions for mesozonal mineralization. *Journal of Structural Geology*, **26**, 1127-1136.

Sperner, B., Müller, B., Heidbach, O., Delvaux D., Reinecker, J. and Fuchs, K. (2003). Tectonic stress in the Earth's crust: advances in the world stress map project. *In:* D.A. Nieuwland (Ed.), *New insights into structural interpretation and modelling*. Geological Society of London Special Publication, **212**, 101-116.

Thiessen, R. (1986). Two-dimensional refold interference patterns. *Journal of Structural Geology*, **8**, 563-573.

Tomkinson, M.J. (1987) *Witkoppies Area – Preliminary Thoughts*. Anglovaal Internal Report (unpubl.), ETC/AVE/87/54, 2pp.

Tomkinson, M.J. (1989) *The Shires Shear Zone, New Consort Gold Mines, Barberton Mountain Land, implications for mine development and mineralization.* Anglovaal Internal Report (unpubl.), ETC/AVE/88/329, 8pp.

Tomkinson, M. J. and Lombard, A. (1990). Structure, metamorphism and mineralization in the New Consort Gold Mines, Barberton Greenstone Belt, South Africa. *In* Glover, J.E., and Ho, SE., (Eds.). *Third International Archaean Symposium, Perth, 1990. Extended Abstracts Volume, Geoconferences (W.A.) Inc., Perth, 377-379.*

Twiss, R.J. and Unruh, J.R. (1998). Analysis of fault slip inversions: Do they constrain stress or strain rate? *Journal of Geophysical Research*, **101**, 8335-8361.

Viljoen, M.J. (1964). *The geology of the Lily syncline and the portion of the Eureka*

syncline between the Consort Mine and Joe's Luck Siding, Barberton Mountain Land. Ph.D. (unpubl.), Univ. Witwatersrand, Johannesburg, 123 pp.

Viljoen, M.J. and Viljoen, R.P., (1969). The geology and geochemistry of the lower ultramafic unit of the Onverwacht Group and proposed new class of igneous rocks: *Special Publication, Geological Society of South Africa*, **2**, 55-86.

Voges, F.D. (1986). The New Consort Gold Mine, Barberton greenstone belt. *In:* C.R. Anhaeusser and S. Maske, (Eds.), *Mineral Deposits of Southern Africa. Vol. 1,* Geological Society of South Africa, Johannesburg, 163-168.

Voges, F.D. (1989). *The PC Shoot*. Anglovaal Internal Report (unpubl.), ETC/AVE/89/64, 3p.

Ward, J.H.W. (1999). The metallogeny of the Barberton Greenstone Belt, South Africa and Swaziland. *Council for Geoscience of South Africa, Memoir* **86**, 108 pp.

Ward, J.H.W. (Compiler) (2000). Metallogenic map of the Barberton Greenstone Belt, South Africa and Swaziland (1:1000 000). *Council for Geoscience Metallogenic Series, Pretoria.*

Figure captions

Figure 1. Geological map of the Jamestown Schist Belt (JSB) showing distribution of rock units transected by thrust faults including: Albion (AF), Woodstock (WF), Lily (LF) and Kaap River (KRF) faults, and gold mines in the study area. The Nelspruit Batholith, Kaap Valley Pluton and Eureka Syncline bound the Jamestown Schist belt (JSB). The inset shows the locality of the JSB in the Barberton Greenstone Belt (BGB) and the position of the Saddleback (SF), Inyoka (IF) and Lily (LF) faults.

Figure 2. Geological map of the New Consort Gold Mine area showing the positions and names of major gold workings (1-8). Grid blocks on the map are 1000m wide.

Figure 3. Map showing anticlines, synclines and fold axial traces formed during the main deformation events described in the text.

Figure 4. Outcrop and thin section photographs of important geological features in the New Consort Gold Mine area. (**a**) An example of a bedding (S_0) - cleavage (S_{1NC}) relationship in greywacke of the Fig Tree Group (GR 307514-7161018); (**b**) Mylonitic pegmatite along the Consort Bar (GR 307258-7162074). Mica-fish and C-S structures show a top to the NW sense of movement; (**c**) Folded ultra-mylonitic pegmatite along the Consort Bar (GR 307385-7162560); (**d**) Elongated conglomerate pebbles in Moodies Group sediments define L_{3NC} (GR 305437-7161281); (**e**) A mineralized, D_{4NC} shear zone, cross-cuts steeply dipping sandstone (see Figures 2 and 10 for old workings locations); (**f**) Mineralized D_{4NC} shear zone cross-cutting talc-schist in the Albion Gold Mine (GR 302120-7160337); (**g**) D_{4NC} shear fractures crosscut the complexly folded Consort Bar, gold workings have been developed parallel to the fractures (GR 307348-7162505); (**h**) Slickensided surface with quartz fibre growth on a D_{4NC} fault indicating a normal sense of movement (MRC ore body at 24 level in Sheba Mine).

Figure 5. Map of the triple junction showing a network of major D_{3NC} shear zones, and associated orientations of mylonitic lineations (L_{3aNC}) indicated by arrows. Solid triangles point towards the block that has moved upwards along the shear zones.

Figure 6. Map showing the dome-crescent-mushroom (Type 2) fold interference pattern dominating outcrops around NCGM. Orientation diagrams are presented of folded shear planes (S_{3aNC}) and mylonitic lineations (L_{3aNC}) developed during $D_{3a\ NC}$. Fold axial planes and fold axes for D_{3bNC} and D_{3cNC} structures are indicated. A and B represent structural domains on either side of the main D_{3cNC} fold, and 1, 2 and 3 indicate sub-domains defined by the limbs of D_{3bNC} folds with the respective orientation data presented on equal area projection.

Figure 7. Stereo plots of (**a**) orientations of fold axes ($F_{3b,c\ NC}$) collected from a zone that records interference folding between D_{3bNC}, and D_{3cNC} folds, and (**b**) Pebble elongation directions (L_{3cNC}) collected from agglomerate and conglomerate in the core of a D_{3cNC} fold, between domain A3 and B1 in figure 6.

Figure 8. Stereo plots of the results of the optimized right dihedron method using TENSOR (Delvaux and Sperner, 2003). For all sites a plot of the fault planes and slip vectors is provided together with the orientation of the principle stress axes (S1 – S3), the principle horizontal stress axis (σhmin = open arrows; σhmax = closed arrows) and a histogram of deviation angles (α). A measure of the input data quality (QRw and QRt), stress regime (R) and homogeneity of the dataset (F5) is also provided. Locations of individual workings are shown in Figure 2. Results are summarized in Table 2a and 2b.

Figure 9. Map of the Mine Manager Quarry (Figure 2) along the complexly folded Consort Bar. Inserts include a plot of mineralized fractures and averaged trends of σ_1 (open arrows) and σ_3 (closed arrows).

Figure 10. Map of WNW, NNW and ENE trending D_{4NC} fracture corridors along which mineralisation is concentrated. (**a**) Stereo plots of mineralized fracture planes with slip

vectors pointing towards the movement direction of the hanging wall, (**b**) stress diagrams calculated using TENSOR showing σhmin = open arrows; σhmax = green arrows) (**c**) Bingham, fault slip inversions for palaeo-stress shown as 'beach balls' (grey areas for tension dihedrons)

Figure 11. Map of mineralized corridors, gold workings and brittle-ductile shear fractures in Clutha, Woodstock and Albion Mines (grid spacing is 100m). (**a**) Stereo plots of mineralized fracture planes with slip vectors pointing towards the movement direction of the hanging wall, (**b**) stress diagrams calculated using TENSOR showing σhmin = open arrows; σhmax = green arrows) (**c**) Bingham, fault slip inversions for palaeo-stress shown as 'beach balls' (grey areas for tension dihedrons).

Table 1. Summary of the major geological events affecting the Barberton greenstone belt (after de Ronde and de Wit, 1994), with a comparison to more locally relevant deformation schemes proposed by Lowe *et al.* (1999), Dirks et al. (2009), Anhaeusser (1976), Viljoen (1964), Tomkinson and Lombard (1990) and Harris et al. (1995). To prevent confusion, the subscript "NC" for 'New Consort' has been added to the deformation scheme proposed in this study.

Table 2(a). Summary of results from fault slip inversion for palaeo-stress by calculating a linked Bigham fault plane solution using FaultKin (Allmendinger, 2001). Eigenvalues (ev) for the calculated moment tensors have been used to obtain a stress ratio (Rev = [ev2-ev3]/[ev1-ev3])., (σ) represents stress axis and Rev′ is an adjusted stress ratio (see text for explanation) to estimate the stress regime. Refer to figures 10 and 11 for localities of mineralised corridors.

Table 2(b). Summary of results from fault slip inversion for palaeo-stress by using the optimized, iterative, right dihedron approach in TENSOR after Delvaux and Sperner (2003). 'nt' is the total number of measurements; 'n/nt' the percentage of measurements used in the final calculation and (σ) represents stress axis. The average deviation angle

(α), standard deviation and maximum α angle are given together with an indication of data quality (QRw), stress ration (R) and stress regime (R′). See text for explanation.

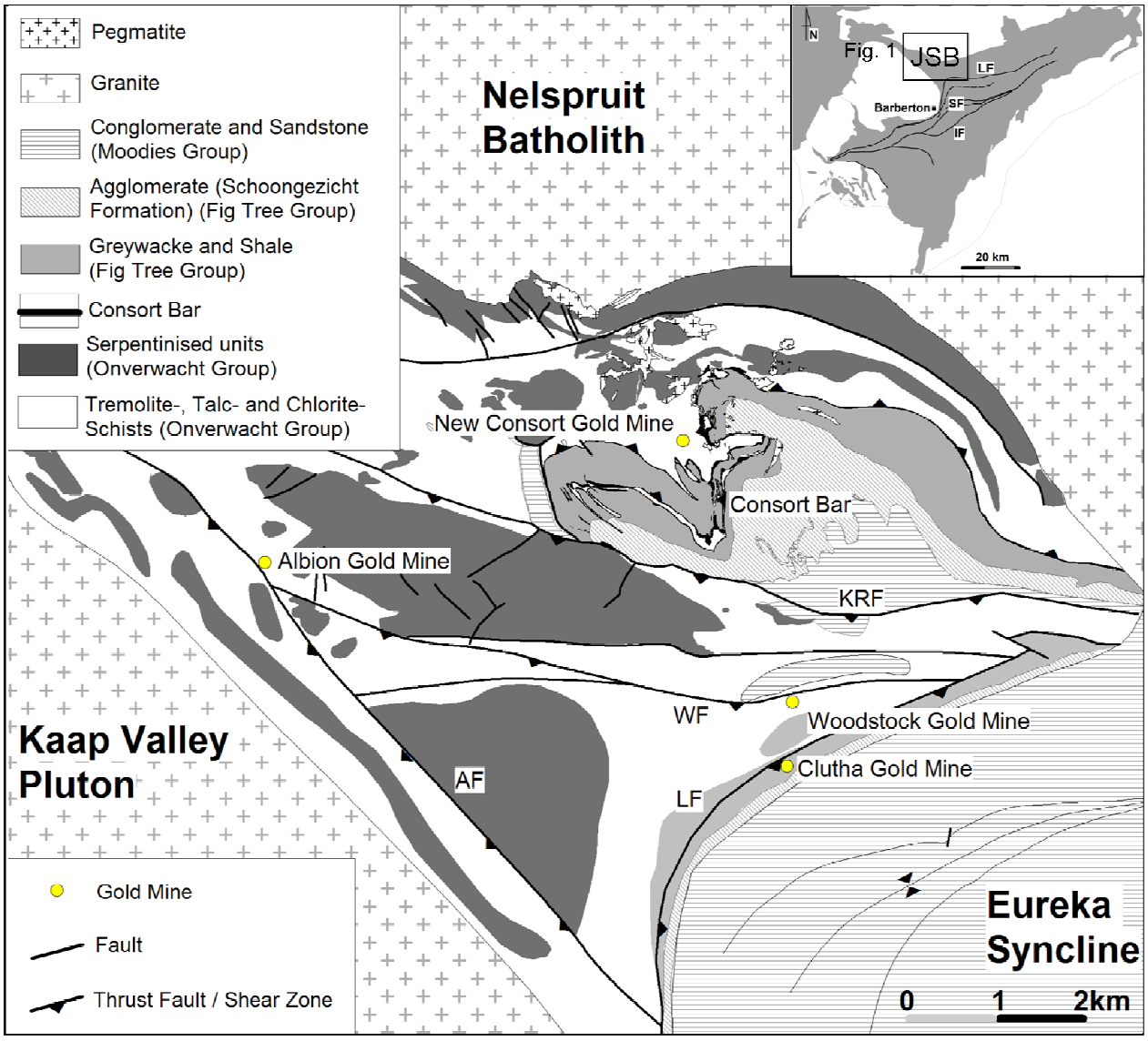
Pegmatite
Granite
Conglomerate and Sandstone (Moodies Group)
Agglomerate (Schoongezicht Formation) (Fig Tree Group)
Greywacke and Shale (Fig Tree Group)
Consort Bar
Serpentinised units (Onverwacht Group)
Tremolite-, Talc- and Chlorite-Schists (Onverwacht Group)
Nelspruit Batholith
N
Fig. 1
JSB
LF
Barberton
SF
IF
20 km
New Consort Gold Mine
Consort Bar
Albion Gold Mine
KRF
WF
Woodstock Gold Mine
Clutha Gold Mine
Kaap Valley Pluton
AF
LF
Eureka Syncline
Gold Mine
Fault
Thrust Fault / Shear Zone
0
1
2km

Figure 1

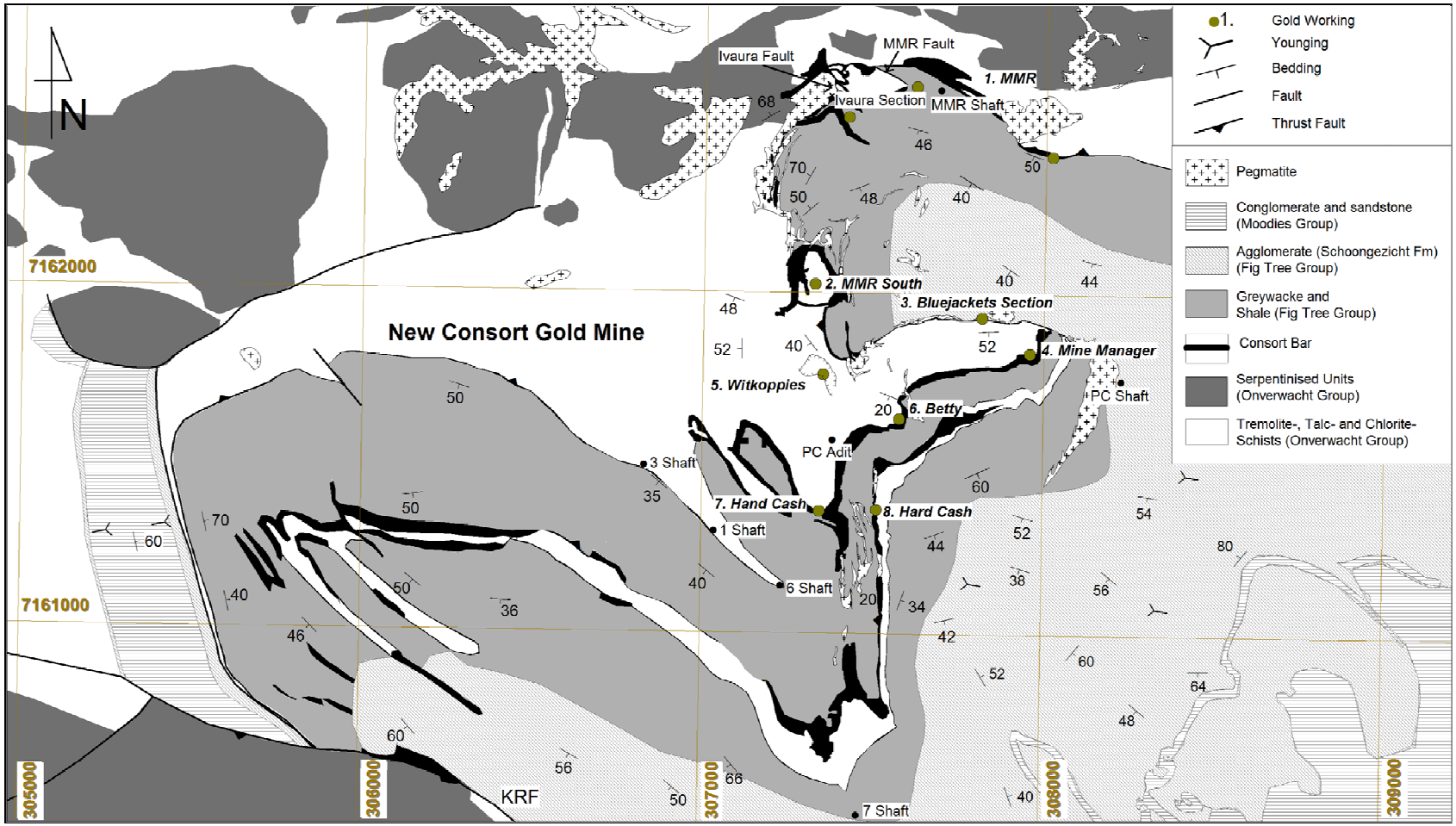
N
New Consort Gold Mine
Ivaura Fault
MMR Fault
1. MMR
Ivaura Section
MMR Shaft
2. MMR South
3. Bluejackets Section
4. Mine Manager
5. Witkoppies
6. Betty
PC Shaft
PC Adit
3 Shaft
7. Hand Cash
8. Hard Cash
1 Shaft
6 Shaft
7 Shaft
KRF
7162000
7161000
305000
306000
307000
308000
309000
1. Gold Working
Younging
Bedding
Fault
Thrust Fault
Pegmatite
Conglomerate and sandstone (Moodies Group)
Agglomerate (Schoongezicht Fm) (Fig Tree Group)
Greywacke and Shale (Fig Tree Group)
Consort Bar
Serpentinised Units (Onverwacht Group)
Tremolite-, Talc- and Chlorite-Schists (Onverwacht Group)

Figure 2

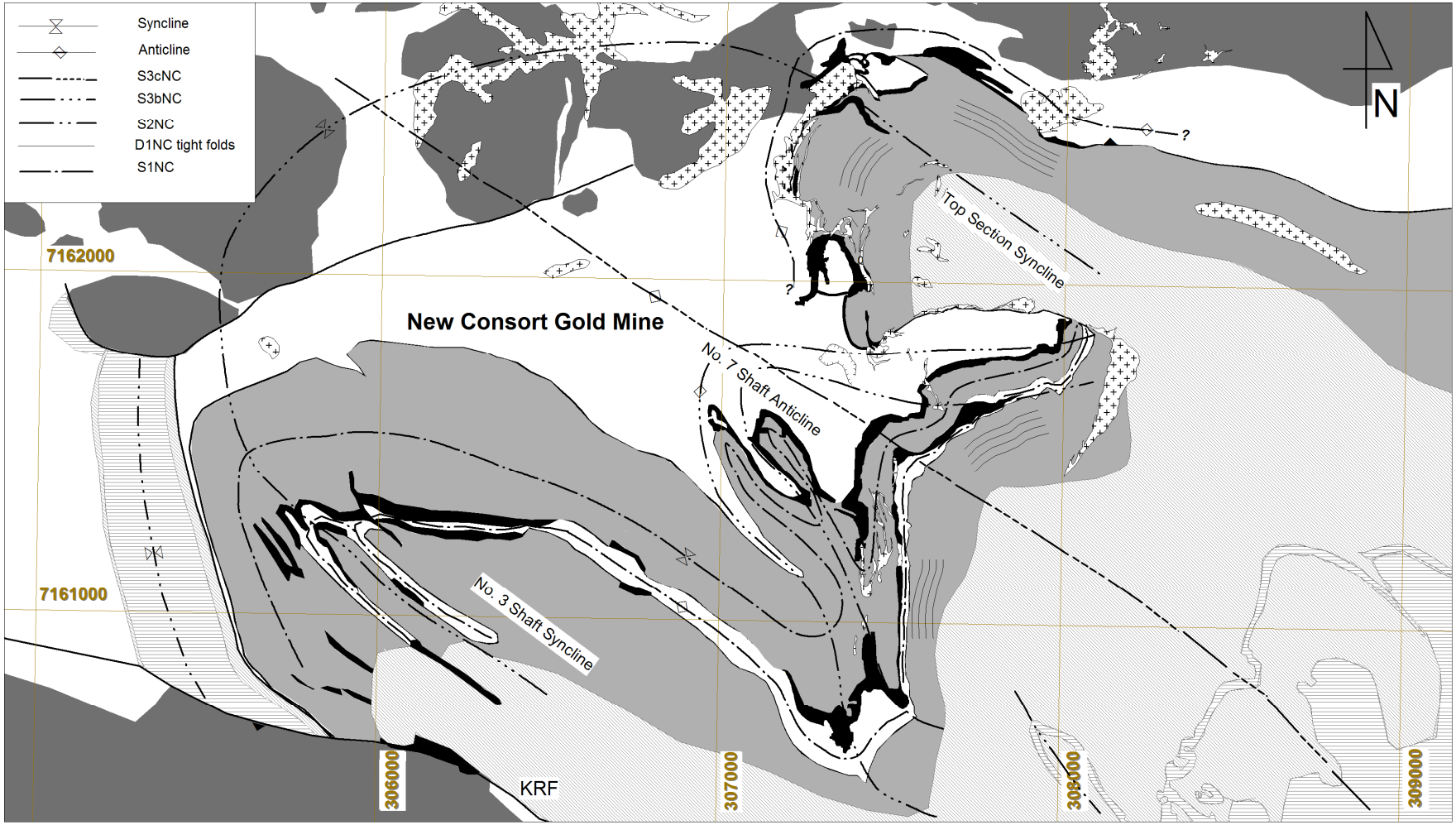
Syncline
Anticline
S3cNC
S3bNC
S2NC
D1NC tight folds
S1NC
N
7162000
7161000
New Consort Gold Mine
Top Section Syncline
No. 7 Shaft Anticline
No. 3 Shaft Syncline
KRF
306000
307000
308000
309000

Figure 3

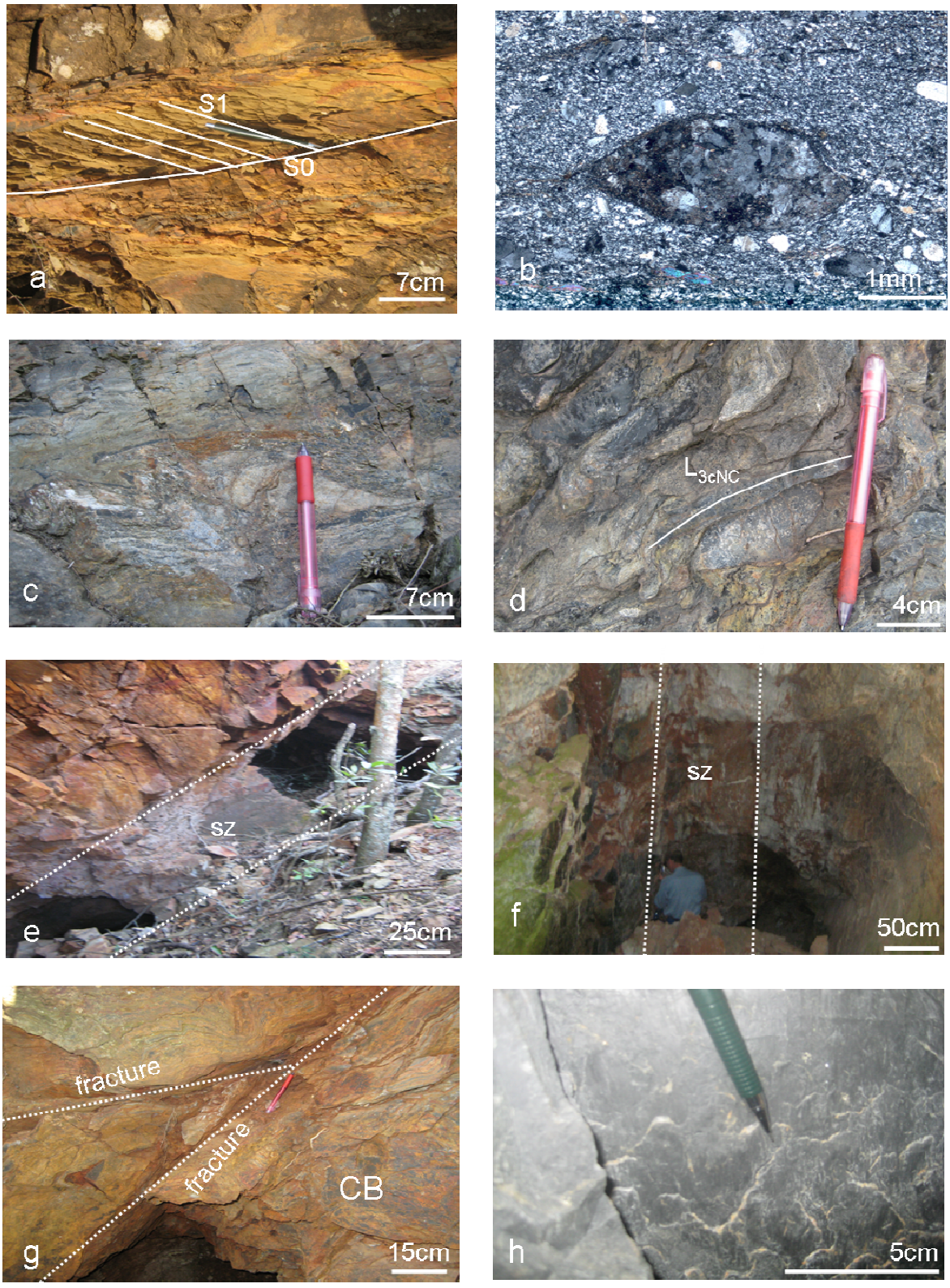
S1
S0
a
7cm
b
1mm
c
7cm
L_{3cNC}
d
4cm
sz
e
25cm
sz
f
50cm
fracture
fracture
CB
g
15cm
h
5cm

Figure 4

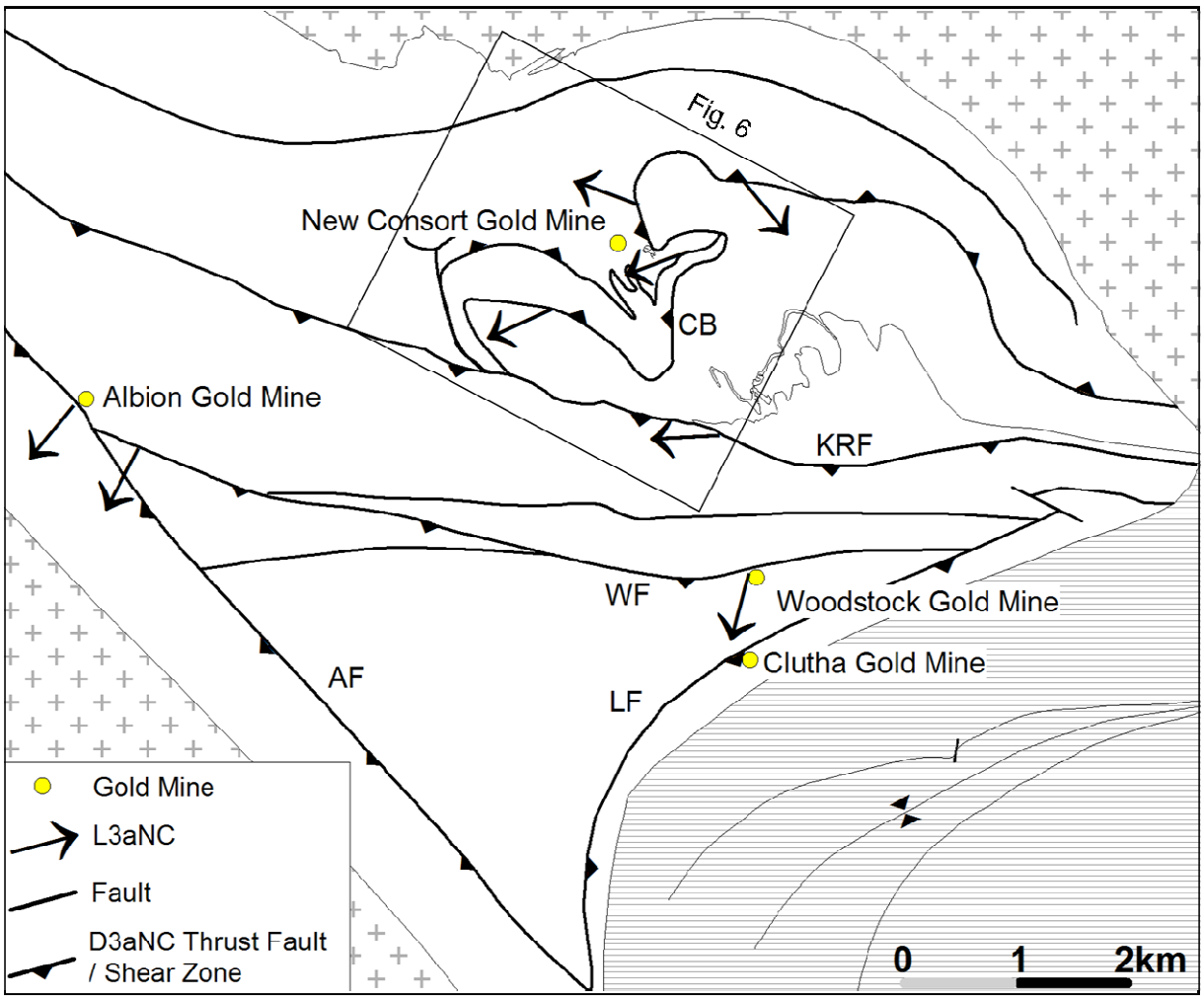
Fig. 6
New Consort Gold Mine
CB
Albion Gold Mine
KRF
WF
Woodstock Gold Mine
Clutha Gold Mine
AF
LF
Gold Mine
L3aNC
Fault
D3aNC Thrust Fault / Shear Zone
0
1
2km

Figure 5

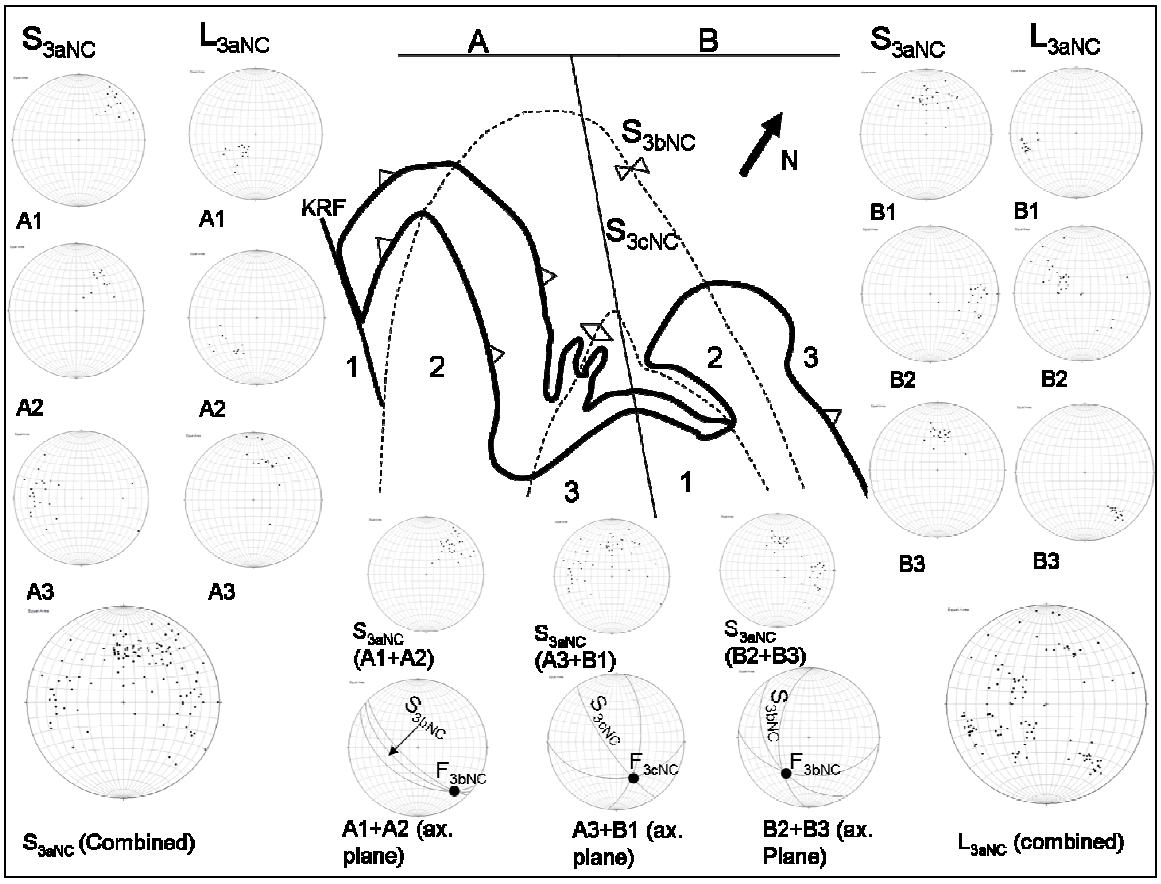

Figure 6

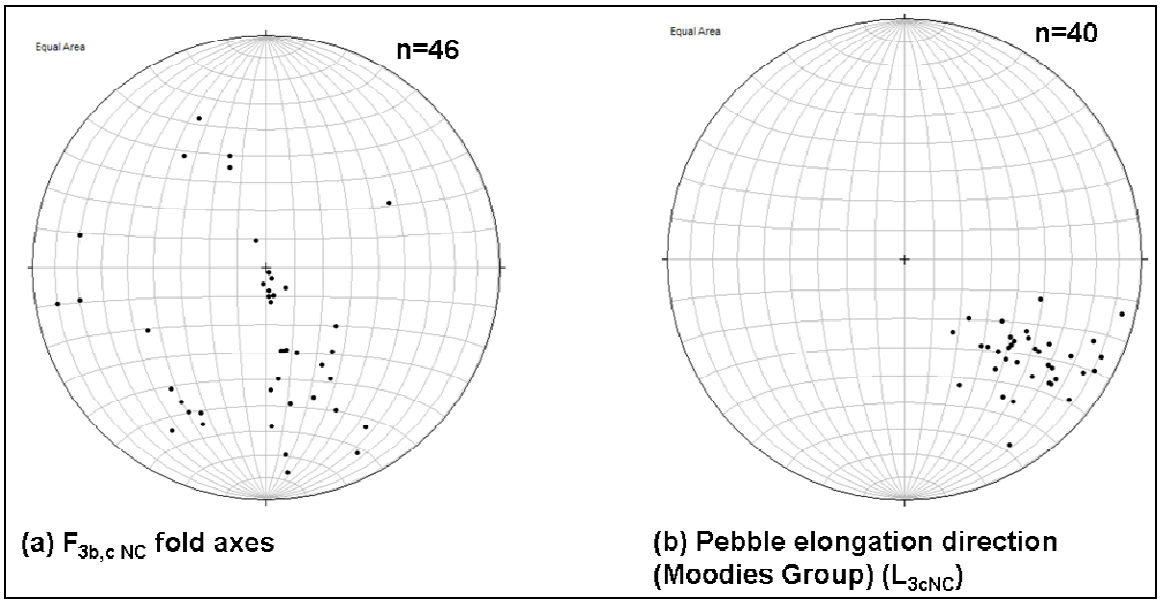

Figure 7

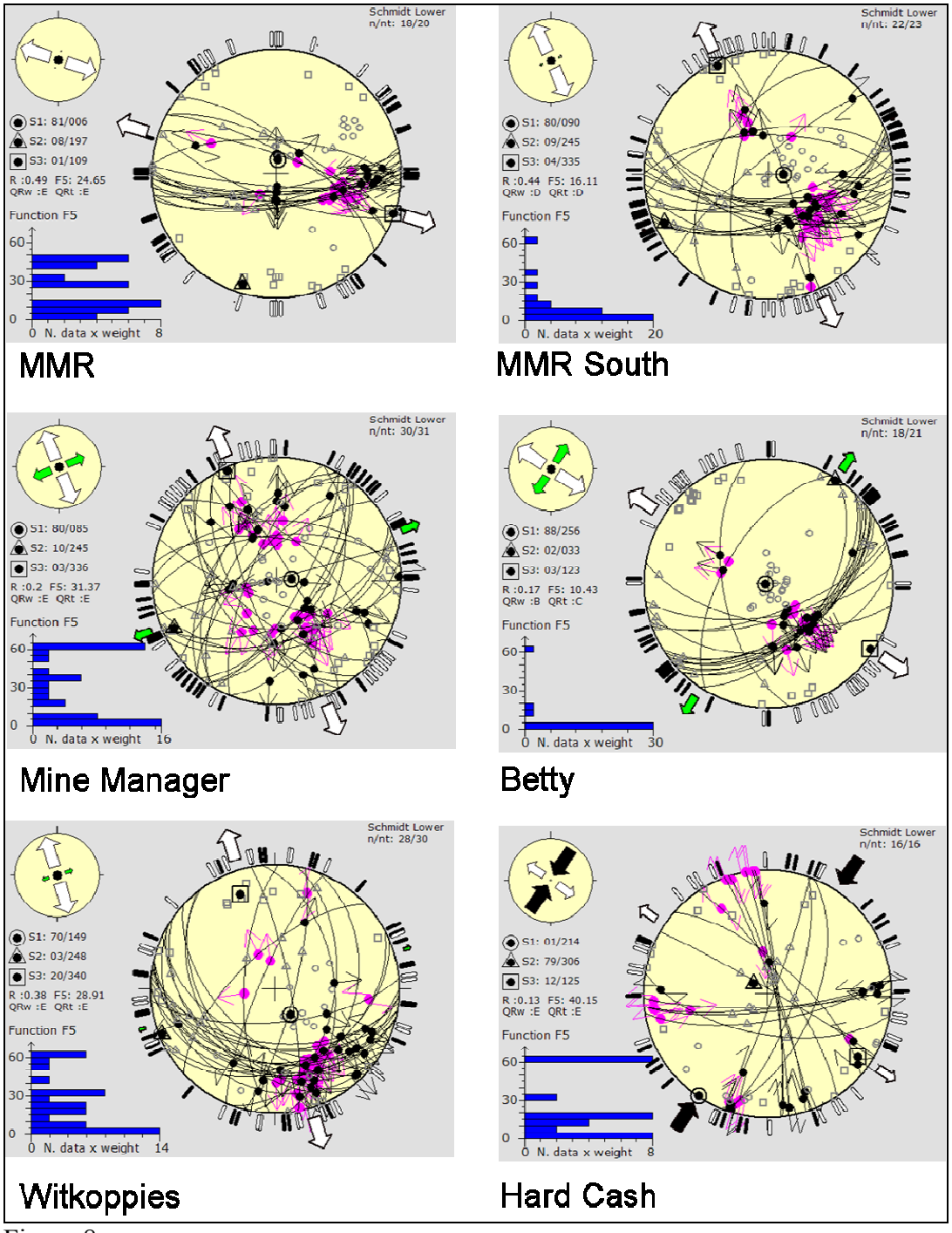
Schmidt Lower
n/nt: 18/20
S1: 81/006
S2: 08/197
S3: 01/109
R :0.49 F5: 24.65
QRw :E QRt :E
Function F5
60
30
0
0 N. data x weight 8
MMR
Schmidt Lower
n/nt: 22/23
S1: 80/090
S2: 09/245
S3: 04/335
R :0.44 F5: 16.11
QRw :D QRt :D
Function F5
60
30
0
0 N. data x weight 20
MMR South
Schmidt Lower
n/nt: 30/31
S1: 80/085
S2: 10/245
S3: 03/336
R :0.2 F5: 31.37
QRw :E QRt :E
Function F5
60
30
0
0 N. data x weight 16
Mine Manager
Schmidt Lower
n/nt: 18/21
S1: 88/256
S2: 02/033
S3: 03/123
R :0.17 F5: 10.43
QRw :B QRt :C
Function F5
60
30
0
0 N. data x weight 30
Betty
Schmidt Lower
n/nt: 28/30
S1: 70/149
S2: 03/248
S3: 20/340
R :0.38 F5: 28.91
QRw :E QRt :E
Function F5
60
30
0
0 N. data x weight 14
Witkoppies
Schmidt Lower
n/nt: 16/16
S1: 01/214
S2: 79/306
S3: 12/125
R :0.13 F5: 40.15
QRw :E QRt :E
Function F5
60
30
0
0 N. data x weight 8
Hard Cash

Figure 8

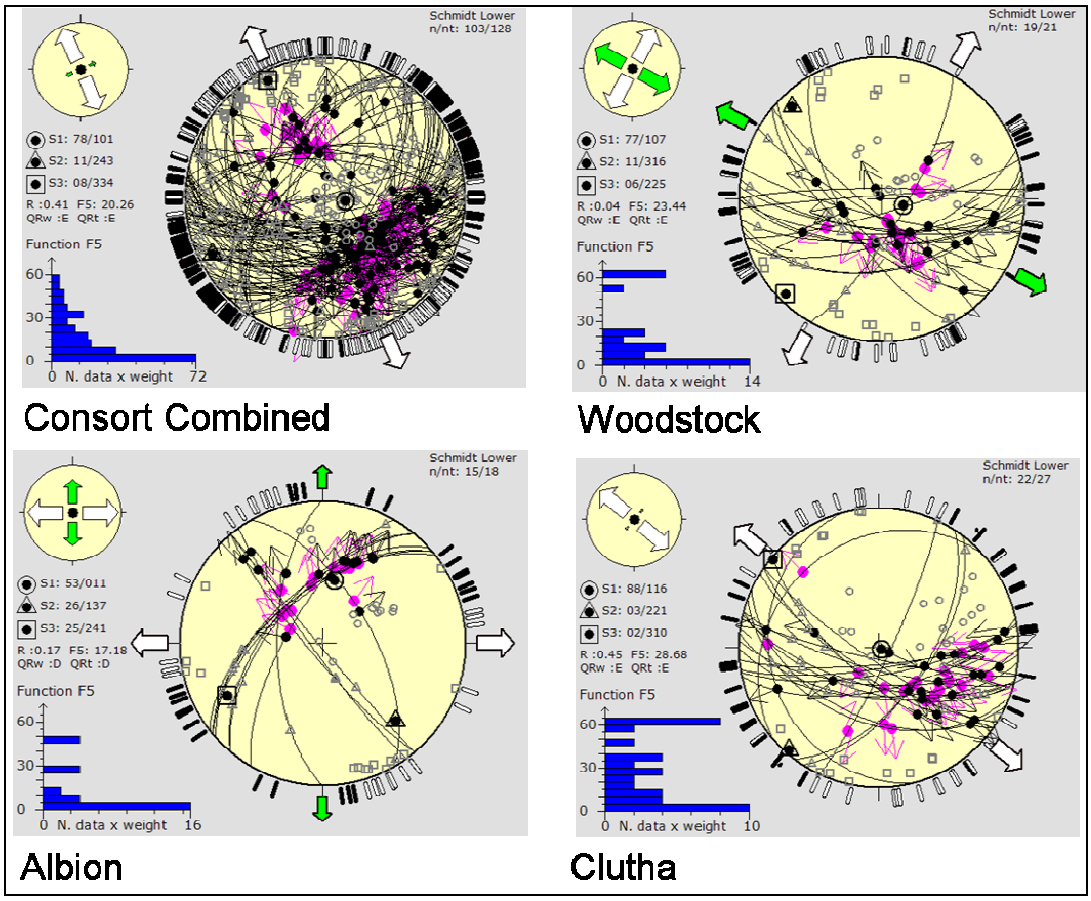

Figure 8 continue

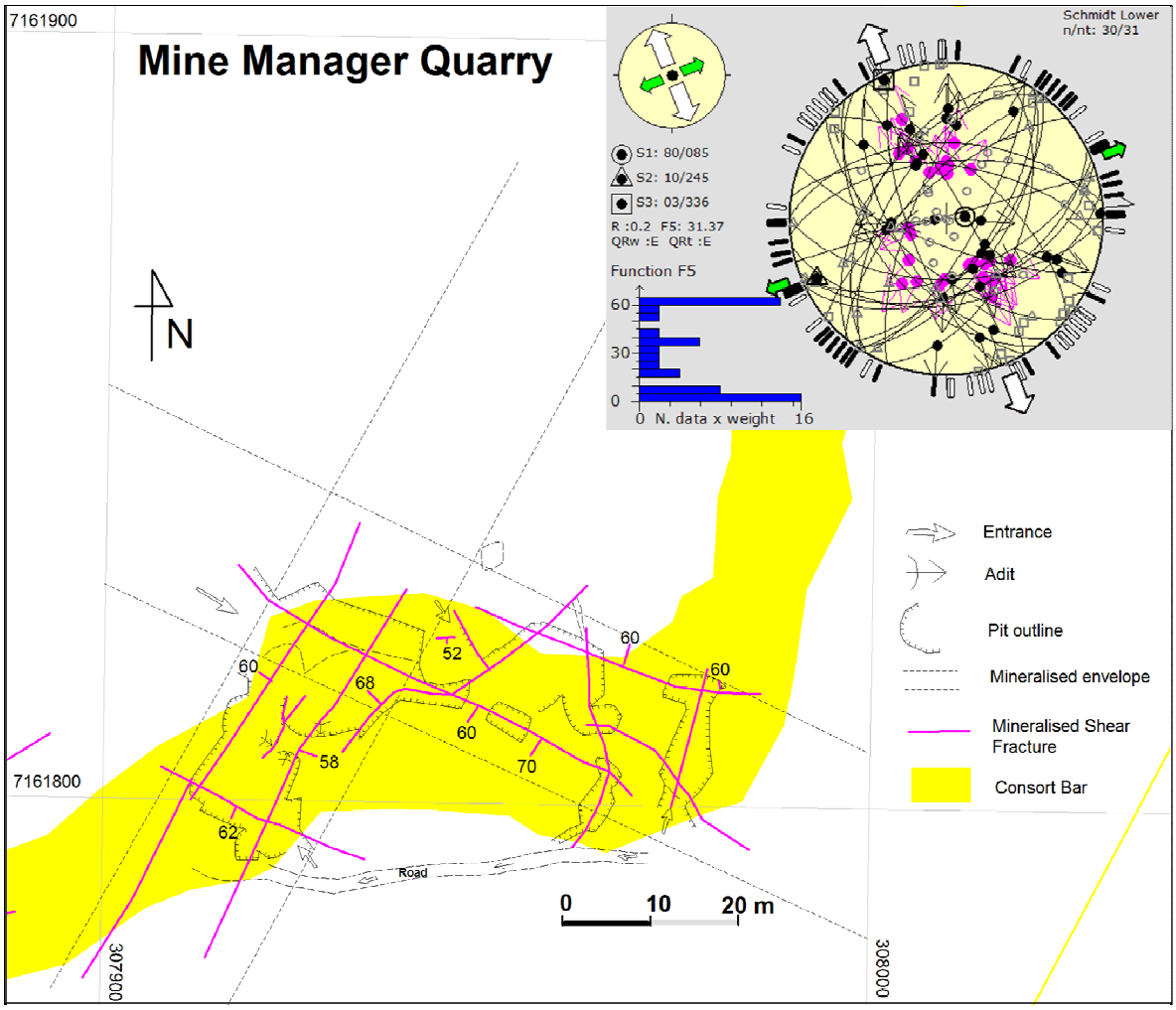
7161900
Mine Manager Quarry
N
Schmidt Lower
n/nt: 30/31
S1: 80/085
S2: 10/245
S3: 03/336
R :0.2 F5: 31.37
QRw :E QRt :E
Function F5
60
30
0
0 N. data x weight 16
Entrance
Adit
Pit outline
Mineralised envelope
Mineralised Shear Fracture
Consort Bar
60
60
52
68
60
58
70
60
62
Road
7161800
0 10 20 m
307900
308000

Figure 9

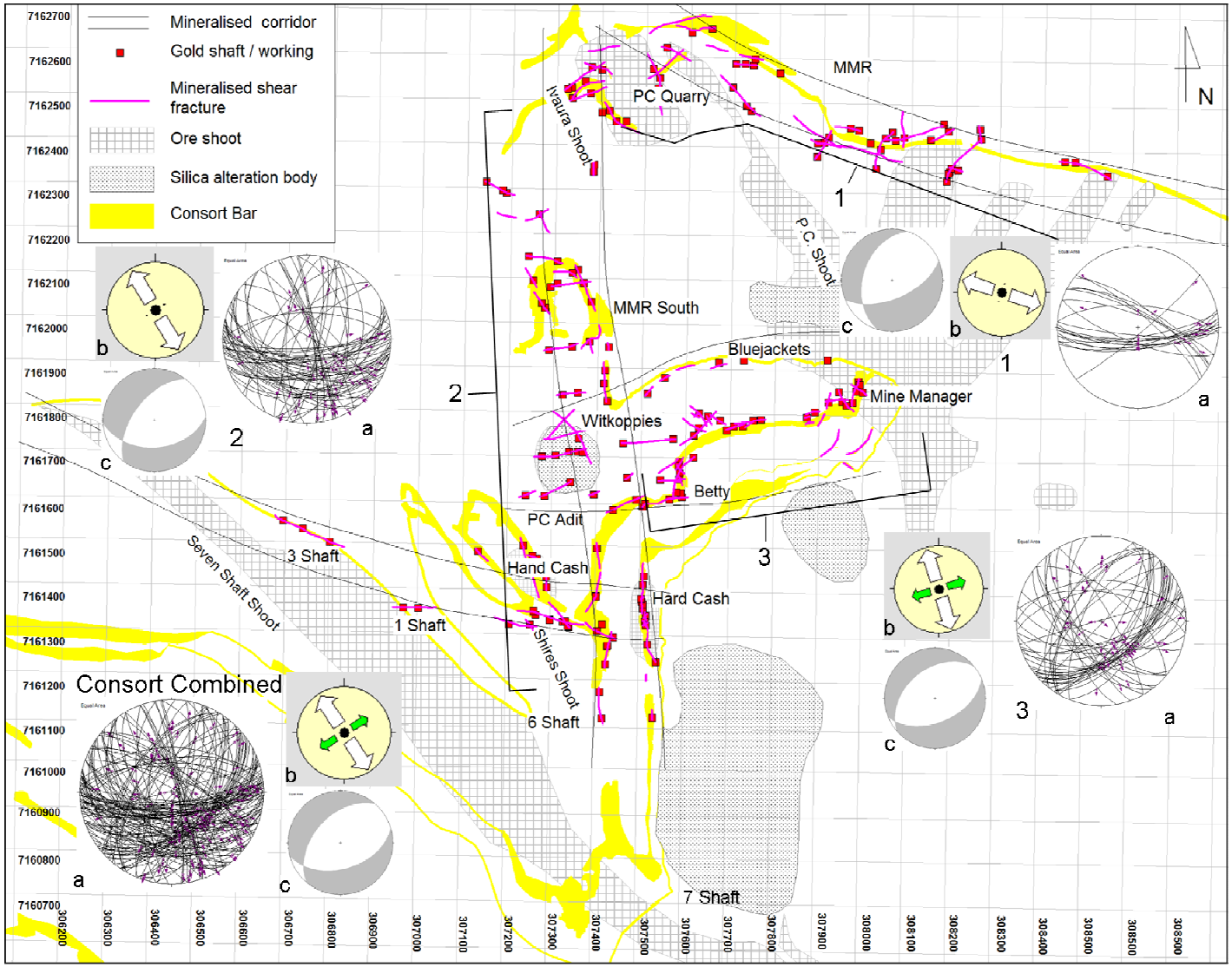
Mineralised corridor
Gold shaft / working
Mineralised shear fracture
Ore shoot
Silica alteration body
Consort Bar
MMR
PC Quarry
Maura Shoot
P.C. Shoot
MMR South
Bluejackets
Mine Manager
Witkoppies
Betty
PC Adit
3 Shaft
Hand Cash
Hard Cash
Seven Shaft Shoot
1 Shaft
Shires Shoot
6 Shaft
7 Shaft
Consort Combined
N
1
2
3
a
b
c

Figure 10

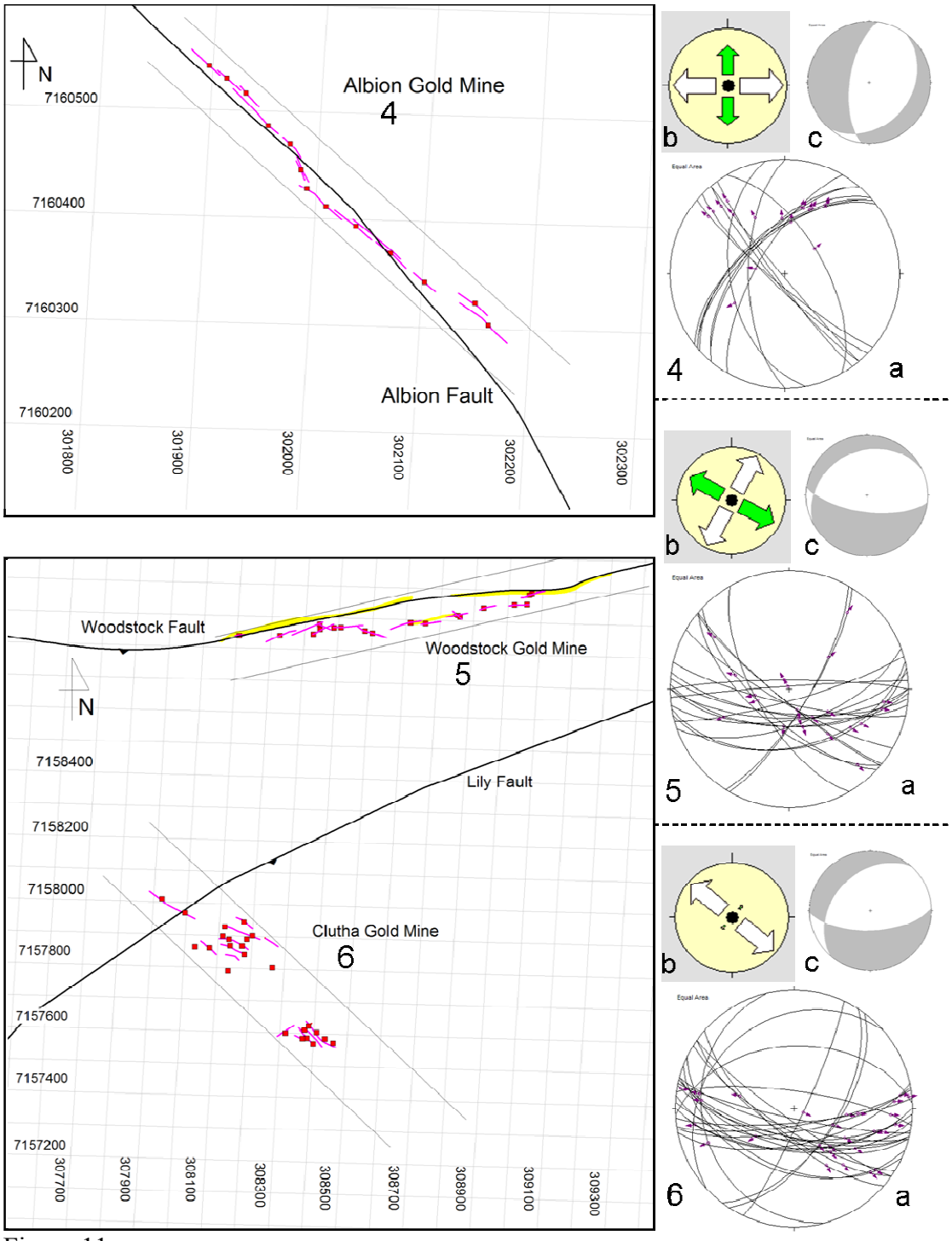
N
Albion Gold Mine
4
Albion Fault
7160500
7160400
7160300
7160200
301800
301900
302000
302100
302200
302300
b
c
4
a
Woodstock Fault
Woodstock Gold Mine
5
N
Lily Fault
7158400
7158200
7158000
7157800
7157600
7157400
7157200
Clutha Gold Mine
6
307700
307900
308100
308300
308500
308700
308900
309100
309300
5
6

Figure 11

Tectonic event description (after de Ronde and de Wit, 1994)		de Ronde & de Wit (1994) ***Regional***	Lowe et al. (1999) ***South of Barberton Town***	Ramsay (1963) & Anhaeusser (1976) ***Sheba Hills***	Dirks et al. (2009) ***Sheba Hills***	Viljoen (1964) ***Consort Area***	Harris et al. (1995) ***Consort Area***	This study
Formation of oceanic crust; ocean floor type metamorphism (~3.55 Ga)	Deposition of Lower Onverwacht Group	D_0						
Subduction-accretion of immature island arc systems (3.55-3.45 Ga)	Deposition of Lower Onverwacht Group	D_1						
Subduction-accretion in a Cordillearan-type subduction system (3.26-3.22 Ga)	Accretion of Upper Onverwacht Group and deposition of Fig Tree Group	D_2	D_2 Folding of Onverwacht and Fig Tree rocks	D_{1s} Folding and thrusting of Onverwacht Fig Tree and Moodies Groups	D_{1s} Folding of the Onverwacht and Fig Tree Groups. Development of S1	D_1 Folding and thrusting of Onverwacht, Fig Tree and Moodies Group. Formation of Lily Syncline	D_1 Recumbent isoclinal folds and tectonic slides. Development of S1 cleavage	D_{1NC} Folding of the Onverwacht and Fig Tree Groups. Development of S_{1NC}
Terrain accretion and deposition of coarse clastics, with collisional amalgamation followed by transcurrent faulting (3.26-3.16)	Deposition of Moodies Group sediments	Early D_3	D_3 Thrusting of Moodies onto Fig Tree D_4 Folding of Moodies Group D_{5a} Upright folding D_{5b} Emplacement of Kaap Valley pluton and foliation development	D_{2s} Formation of regional cleavage with emplacement of Kaap Valley pluton	Late D_{1s} Deposition of the Moodies Group D_{2s} Folding of the Moodies Group and development of Eureka Syncline	D_2 Formation of regional cleavage with emplacement of Kaap Valley pluton		Late D_{1NC} Deposition of the Moodies Group D_{2NC} Folding of the Moodies Group and development of Eureka Syncline
Gold mineralization; shift from transpression to transtensional deformation (~3.1 Ga)	Deposition of Moodies Group sediments	Late D_3	D_{5c} Refolding	D_{3s} Refolding Eureka syncline with dextral thrusting on Sheba fault followed by gold mineralization	D_{4s} Normal faulting Gold Mineralisation	D_3 Refolding of the SW plunging folds such as the Lily Syncline Formation of Consort SE plunging folds. Gold Mineralisation	D_2 Development of north-south to NW-SE trending vertically dipping shear zones Development of SSZ Intrusion of Consort pegmatites. Later NW-SE trending SW dipping faults displacing ore shoots. Dextral strike-slip faults.	D_{4NC} Normal faulting Gold Mineralisation
Strike-slip and normal faulting; emplacement of alkaline batholiths (~3.1 Ga)		D_4		D_{4s} Formation of conjugate recumbent crenulation and chevron folds	D_{3s} Refolding of the F2 folds	D_4 Development of intermediate size folds with horizontal fold axial planes, crenulation, conjugate and flat lying kink-bands. Normal faulting	D_3 Normal faults displacing ore shoots.	D_{3NC} Refolding of the F2 folds

Table 1

Mineralised Corridors											
#	**Name**	**n**	**σ 1**	**σ 2**	**σ 3**	**ev1**	**ev2**	**ev3**	**Rev**	**Rev′**	**Stress regime**
NCGM											
1	**WNW** (MMR)	21	027\62	231\26	136\10	-0.2191	-0.0042	0.2233	0.51	0.51	Pure extensional
2	**NNW** (MMR South, Witkoppies and Hard Cash)	70	071\63	237\27	330\06	-0.2566	-0.0367	0.2932	0.60	0.60	Pure extensional
3	**ENE** (Mine Manager and Betty)	54	033\80	240\09	149\04	-0.3429	0.0398	0.3032	0.41	0.41	Pure extensional
	Consort Combined	145	057\72	238\17	148\04	-0.2673	-0.0112	0.2785	0.53	0.53	Pure extensional
Outside NCGM											
4	Albion	18	069\68	194\13	289\17	-0.3054	0.0582	0.2471	0.34	0.34	Radial extensional
5	Woodstock	21	032\65	272\13	176\21	-0.3011	0.0894	0.2117	0.24	0.24	Radial extensional
6	Clutha	27	041\63	255\23	160\14	-0.2560	0.0198	0.2362	0.44	0.44	Pure extensional

Table 2a

Mineralised Corridors															
#	**Name**	**nt**	**n/nt**	**σ 1**	**σ 2**	**σ 3**	**α**	**QRw**	**σhmax**	**σhmin**	**Std. Dev**	**Max.**	**R**	**R′**	**Stress regime**
NCGM															
1	**WNW** (MMR)	21	0.9	006\81	197\08	109\01	24.65	E	018	108	13	42.8	0.49	0.49	Pure extensional
2	**NNW** (MMR South, Witkoppies and Hard Cash)	70	0.99	091\73	236\14	327\09	31.14	E	059	149	31.3	176.6	0.54	0.54	Pure extensional
3	**ENE** (Mine Manager and Betty)	54	0.98	087\81	252\09	342\01	22.83	E	074	164	21.99	81.7	0.16	0.16	Radial extension
	Consort Combined	144	0.94	111\83	228\03	318\06	27.63	E	049	139	21.93	84.1	0.31	0.31	Pure extensional
Outside NCGM															
6	Albion	18	083	011\53	137\26	241\25	17.8	D	180	90	13.77	43.3	0.17	0.14	Radial extensional
7	Woodstock	21	0.9	107\77	316\11	255\06	23.44	D	119	029	19.63	60.3	0.04	0.04	Radial extensional
8	Clutha	27	0.81	116\88	221\03	310\02	28.68	E	040	130	17.2	95.7	0.45	0.45	Pure extensional

Table 2b